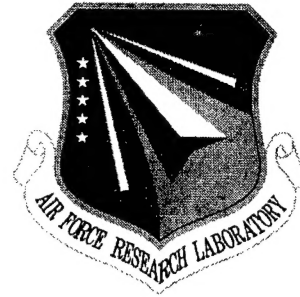


AFRL-IF-RS-TR-2001-159
Final Technical Report
August 2001



CORRELATED HOPPING ENHANCED SPREAD SPECTRUM (CHESS) STUDY

BAE Systems

Sponsored by
Defense Advanced Research Projects Agency
DARPA Order No. K037

APPROVED FOR PUBLIC RELEASE; DISTRIBUTION UNLIMITED.

The views and conclusions contained in this document are those of the authors and should not be interpreted as necessarily representing the official policies, either expressed or implied, of the Defense Advanced Research Projects Agency or the U.S. Government.

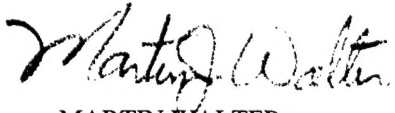
20011005 150

AIR FORCE RESEARCH LABORATORY
INFORMATION DIRECTORATE
ROME RESEARCH SITE
ROME, NEW YORK

This report has been reviewed by the Air Force Research Laboratory, Information Directorate, Public Affairs Office (IFOIPA) and is releasable to the National Technical Information Service (NTIS). At NTIS it will be releasable to the general public, including foreign nations.

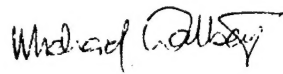
AFRL-IF-RS-TR-2001-159 has been reviewed and is approved for publication.

APPROVED:



MARTIN WALTER
Project Manager

FOR THE DIRECTOR:



MICHAEL L. TALBERT, Technical Advisor
Information Technology Division
Information Directorate

If your address has changed or if you wish to be removed from the Air Force Research Laboratory Rome Research Site mailing list, or if the addressee is no longer employed by your organization, please notify AFRL/IFTC, 26 Electronic Pky, Rome, NY 13441-4514. This will assist us in maintaining a current mailing list.

Do not return copies of this report unless contractual obligations or notices on a specific document require that it be returned.

CORRELATED HOPPING ENHANCED SPREAD SPECTRUM
(CHESS) STUDY

Diane Mills

Contractor: BAE Systems
Contract Number: F30602-00-C-0157
Effective Date of Contract: 29 June 2000
Contract Expiration Date: 26 February 2001
Short Title of Work: Correlated Hopping Enhanced Spread
Spectrum (CHESS) Study
Period of Work Covered: Jun 00 - Feb 01

Principal Investigator: Diane Mills
Phone: (603) 885-3141
AFRL Project Engineer: Martin Walter
Phone: (315) 330-4102

APPROVED FOR PUBLIC RELEASE; DISTRIBUTION
UNLIMITED.

This research was supported by the Defense Advanced Research
Projects Agency of the Department of Defense and was monitored
by Martin Walter, AFRL/IFTC, 26 Electronic Pky, Rome, NY.

REPORT DOCUMENTATION PAGE			Form Approved OMB No. 0704-0188	
Public reporting burden for this collection of information is estimated to average 1 hour per response, including the time for reviewing instructions, searching existing data sources, gathering and maintaining the data needed, and completing and reviewing the collection of information. Send comments regarding this burden estimate or any other aspect of this collection of information, including suggestions for reducing this burden, to Washington Headquarters Services, Directorate for Information Operations and Reports, 1215 Jefferson Davis Highway, Suite 1204, Arlington, VA 22202-4302, and to the Office of Management and Budget, Paperwork Reduction Project (0704-0188), Washington, DC 20503.				
1. AGENCY USE ONLY (Leave blank)		2. REPORT DATE AUGUST 2001		3. REPORT TYPE AND DATES COVERED Final Jun 00 - Feb 01
4. TITLE AND SUBTITLE CORRELATED HOPPING ENHANCED SPREAD SPECTRUM (CHES) STUDY			5. FUNDING NUMBERS C - F30602-00-C-0157 PE - 63760E PR - CHES TA - S0 WU - 01	
6. AUTHOR(S) Diane Mills				
7. PERFORMING ORGANIZATION NAME(S) AND ADDRESS(ES) BAE Systems P.O. Box 868 MER15-2222 Nashua NH 03061-0868			8. PERFORMING ORGANIZATION REPORT NUMBER N/A	
9. SPONSORING/MONITORING AGENCY NAME(S) AND ADDRESS(ES) Defense Advanced Research Projects Agency Air Force Research Laboratory/IFTC 3701 North Fairfax Drive 26 Electronic Pky Arlington VA 22203-1714 Rome New York 13441-4514			10. SPONSORING/MONITORING AGENCY REPORT NUMBER AFRL-IF-RS-TR-2001-159	
11. SUPPLEMENTARY NOTES Air Force Research Laboratory Project Engineer: Martin Walter/IFTC/(315) 330-4102				
12a. DISTRIBUTION AVAILABILITY STATEMENT APPROVED FOR PUBLIC RELEASE; DISTRIBUTION UNLIMITED.			12b. DISTRIBUTION CODE	
13. ABSTRACT (Maximum 200 words) This report describes a study to identify and quantify the advantages of Correlated Hopping Enhanced Spread Spectrum (CHES) and enhanced-CHES in the presence of Additive White Gaussian Noise and fading channels. Performance is compared to Direct Sequence Spread Spectrum and fixed frequency hopped methods.				
14. SUBJECT TERMS Frequency Hopping Communication, Fading Channel			15. NUMBER OF PAGES 60	
			16. PRICE CODE	
17. SECURITY CLASSIFICATION OF REPORT UNCLASSIFIED	18. SECURITY CLASSIFICATION OF THIS PAGE UNCLASSIFIED	19. SECURITY CLASSIFICATION OF ABSTRACT UNCLASSIFIED	20. LIMITATION OF ABSTRACT UL	

TABLE OF CONTENTS

Work Summary	1
Results	3
Introduction	4
Conjectures and Verifications	5
Matlab Simulation Results	19
Conclusion	22
References	24
APPENDIX A: Performance Measures	25
APPENDIX B: Communications Bit Error Performance	26
APPENDIX C: Intercept Performance In AWGN	38
Notation/Acronyms	45

LIST OF FIGURES

Figure 1.	Radiometer Processing Block Diagram	6
Figure 2.	Optimum Multichannel FH Pulse Matched ED Processing Block Diagram	6
Figure 3.	BPSK DSSS Performance in Pulsed-Noise Jamming	10
Figure 4.	Comparison of CHESS and TCM Energy Efficiencies	11
Figure 5.	Maximum Number of CHESS Conferenced Users	12
Figure 6.	Number of Correctable Consecutive CHESS Missed Hops	13
Figure 7.	Missed Hop Correction Example for Hop Set Size of 8 and One BPH	14
Figure 8.	Convolutional Code Trellis with Error Path	14
Figure 9.	BPSK DSSS Performance in AWGN with a 10dB NB Jammer	16
Figure 10.	SD CHESS ($M = 64$) Performance in AWGN	17
Figure 11.	CHESS Matlab Simulation Block Diagram	19
Figure 12.	HD CHESS ($M = 16$) Simulation Results	20
Figure 13.	HD CHESS ($M = 64$) Simulation Results	20
Figure 14.	SD CHESS ($M = 16$) Simulation Results	21
Figure 15.	SD CHESS ($M = 64$) Simulation Results	21
Figure 16.	CHESS outperforms DSSS and FH	22
Figure B1.	BPSK DSSS Performance in AWGN as a Function of SNR per Bit	27
Figure B2.	BPSK DSSS Performance in AWGN (also for NB Jamming)	27
Figure B3.	BPSK DSSS Wide-Band Jamming Function	28
Figure B4.	BPSK DSSS Performance in WB Jamming	28
Figure B5.	BFSK Performance in AWGN	29
Figure B6.	K-ary CHESS Performance in AWGN	29
Figure B7.	Hard Decision CHESS ($M = 16$) Performance in AWGN	30
Figure B8.	Hard Decision CHESS ($M = 64$) Performance in AWGN	30
Figure B9.	Soft Decision CHESS Union Bound ($M = 16$) Performance in AWGN	31
Figure B10.	Soft Decision CHESS Union Bound ($M = 64$) Performance in AWGN	31
Figure B11.	Soft Decision CHESS Union Bound ($M = 16384$) Performance in AWGN	32
Figure B12.	FPSK DSSS Performance in a Rayleigh Fading Channel	33
Figure B13.	BFSK Performance in a Rayleigh Fading Channel	33
Figure B14.	K-ary CHESS Performance in a Rayleigh Fading Channel	34
Figure B15.	Hard Decision CHESS ($M = 64$) Performance in a Rayleigh Fading Channel	34
Figure B16.	Hard Decision CHESS ($M = 1024$) Performance in a Rayleigh Fading Channel	35
Figure B17.	Soft Decision CHESS Union Bound ($M = 16$) Performance in a Rayleigh Fading Channel	35

LIST OF FIGURES (Continued)

Figure B18.	Soft Decision CHES Union Bound ($M = 64$) Performance in a Rayleigh Fading Channel	36
Figure B19.	Soft Decision CHES Union Bound ($M = 1024$) Performance in a Rayleigh Fading Channel	36
Figure B20.	Soft Decision CHES Union Bound ($M = 16384$) Performance in a Rayleigh Fading Channel	37
Figure C1.	Radiometer Probability of Detection for $P_{fa} = 10^{-6}$	39
Figure C2.	Radiometer Signal-to-Noise Power Ratio for $P_{fa} = 10^{-6}$	39
Figure C3.	Radiometer Probability of Detection for $P_{fa} = 10^{-6}$	40
Figure C4.	Radiometer Signal-to-Noise Power Ratio for $P_{fa} = 10^{-3}$	40
Figure C5.	Optimum Multichannel FH Pulse-Matched Energy Detector Probability of Detection for $P_{fa} = 10^{-6}$	41
Figure C6.	Optimum Multichannel FH Pulse-Matched Energy Detector Signal-to-Noise Power Ratio for $P_{fa} = 10^{-6}$	41
Figure C7.	Optimum Multichannel FH Pulse-Matched Energy Detector Probability of Detection for $P_{fa} = 10^{-3}$	42
Figure C8.	Optimum Multichannel FH Pulse-Matched Energy Detector Signal-to-Noise Power Ratio for $P_{fa} = 10^{-3}$	42
Figure C9.	Synchronous Coherent Detector Probability of Detection for $P_{fa} = 10^{-6}$	43
Figure C10.	Synchronous Coherent Detector Signal-to-Noise Power Ratio for $P_{fa} = 10^{-6}$	43
Figure C11.	Synchronous Coherent Detector Probabilitiy of Detection for $P_{fa} = 10^{-3}$	44
Figure C12.	Synchronous Coherent Detector Signal-to-Noise Power Ratio for $P_{fa} = 10^{-3}$	44

LIST OF TABLES

Table 1	Likelihood Ratio Test Detectors LPI Margin Example	7
Table 2.	Free Distance Comparison Between CHES and the $(M, 1, \log_2(M))$ Codes	15
Table 3.	Free Distance Comparison Between CHES and the Plotkin Bound	15
Table B1.	Bit/Symbol Error Probability Formulas	26
Table C1.	Intercept Performance Formulas	38

WORK SUMMARY

The Correlated Hopping Enhanced Spread Spectrum (CHESS) radio is an adaptive, fast frequency-hopping, digital radio technology that has been developed by BAE SYSTEMS (formerly Sanders) through its Independent Research and Development (IR&D) efforts [1]. CHESS achieves the desirable performance features of non-interfering spread spectrum operation, spectral re-use, multipath fading mitigation, and interference resistance.

In CHESS, data is encoded using a technique called differential frequency hopping (DFH). This can be defined in the following manner: Given a data symbol X_N and frequency of the previous hop F_{N-1} , the frequency of the next hop is defined as:

$$F_N = G(F_{N-1}, X_N)$$

where the function G can be viewed as a directed graph whose nodes are frequencies and whose vertices are labeled with data patterns. In CHESS, for a set of M frequencies (the nominal CHESS hop set), the graph will have M nodes, and each node will have some number of vertices $f = 2^k$, where k is the number of bits/hop being coded. The parameter f is called the fanout of the graph because it refers to the number of vertices emanating from each node. For example, for a CHESS system using a hopset size of 16 frequencies to encode 2 bits/hop, each of the 16 nodes in the trellis will have four vertices, one associated with each of the four possible inputs. A block of data is encoded by breaking it into words of k bits, and traversing the graph starting as some random node. This is done by executing a hop at each node to the next frequency specified by that node.

AFRL has commissioned BAE SYSTEMS to conduct a trade study on the CHESS system [1]. The goal of the CHESS study is to *identify* and *quantify* the ways in which a CHESS or CHESS-type waveform outperforms other waveforms, particularly with respect to LPD/LPI/AJ properties. Additionally, enhancements have been proposed, and the effects of those enhancements will be studied. As part of this study, the BAE SYSTEMS team has arrived at a series of conjectures about CHESS which we intend to verify, either analytically or by simulation [2]. This final report presents the results of our efforts to verify the conjectures, lists the conjectures and summarizes the efforts made to verify the conjectures.

A brief summary of the technical progress follows. We have considered CHESS operation in both the added white Gaussian noise (AWGN) channel and the Rayleigh-fading channel. The focus of the study was on analyzing CHESS performance, with simple verification provided via a Matlab simulation. Care was taken to develop results that are independent of frequency band. Preliminary results have been for several of the conjectures previously made. It was shown that CHESS outperforms standard frequency hopping (FH) and direct sequence spread spectrum (DSSS) under a variety of conditions.

- CHESS demonstrates better LPD/LPI than fixed FH.
- CHESS and CDMA over the same BW have the similar LPD/LPI characteristics
- CHESS has better AJ performance than CDMA for NB jammers
- CHESS and CDMA have similar AJ performance for WB jammers
- CHESS performs better than CDMA in presence of repeat jammers
- The overall LPD/LPI performance of CHESS is better than TCM
- CHESS allows conferenced users as a feature of its waveform, i.e. a MAC is not required

- CHESS can correct missed hops and false detections
- Chess has potential for self-synchronization
- Practical implementation of CHESS is easier than CDMA

A more detailed summary of results is contained in the remainder of this report.

Results

The study effort quantified the coding gains possible from a CHESS system as well as provides analyses and simulations to determine the LPI/LPD properties of CHESS and proposed CHESS enhancements. A number of methods and approaches, including previously developed convolutional coding results and multiuser detection results, were applied. To attain the goal of the study, the following tasks were originally proposed.

Task 1.1: Study the implementation details and design impact of *changing the frequency coverage* of the CHESS brassboard.

Task 1.2: Study the issues related to *increasing the hop rate* of the basic CHESS system.

Task 1.3: Study the performance enhancements and impact to the basic CHESS system of increasing the *hop set*.

Task 1.4: Study the application of techniques developed for *error correction codes to the hop patterns*.

Task 1.5: Study the efficacy of *modulating the chip frequencies* as a means of increasing the data carrying capacity of the CHESS system.

Task 1.6: Examine methods for *supporting asynchronous operation and conferencing* with CHESS without the use of a preamble in the message.

Task 1.7: Look at methods of *data packing (multiple concurrent users)* via unique DFH structures for each transmission.

Task 1.8: Study CHESS's *sensitivity to fast follow-on jammers*.

Task 1.9: Evaluate the *computational complexity* of the enhanced CHESS algorithm and we shall consider the effect of the proposed enhancements with regard to practical implementation.

It was recognized that a common theme was contained in the above tests: determine the CHESS performance under a variety of circumstances, and, if possible, compare that performance to other spread spectrum systems. To that end, the following conjectures were developed, which we set out to prove. The effects of the changing parameters, such as hop set size or hop rate were then studied within the context of each conjecture.

Introduction

The methodology employed in this study generated results that were independent of specific system parameters in order to find a universal means for comparison. For example, the communications performance results assume no coding of the transmit waveform. Coding gain can easily be incorporated into the results presented herein.

Several approaches to processing the CHESS waveform at the receiver are considered in this study. K-ary frequency hopping provides a lower bound on the hard decision (HD) CHESS bit error rate (BER) in that the receiver makes hard decisions assuming that the last symbol (bit) is known. M-ary frequency hopping provides an upper bound on the HD CHESS BER in that the receiver makes hard decisions assuming that the last symbol (bit) is not known. The exact HD CHESS probability of a bit error is an exact equation derived in the course of this study. The soft-decision (SD) union bound provides an upper bound on the SD CHESS BER and accounts for use of the trellis to recover missed hops.

All of the CHESS analysis assumes 1 bit per hop unless otherwise specified and the direct sequence spread spectrum (DSSS) is of the BPSK-BPSK type with the communications bandwidth exactly equal to the inverse of the chip rate, i.e. $WT_c = 1$. The processing gain (PG) for all of the waveforms considered is the ratio of the signal bandwidth to the data bandwidth (W/R_b), which is equivalent to the ratio of the bit duration to the chip duration (T_b/T_c) for BPSK DSSS. Therefore, the given value for PG implies the “spread” of the system under consideration. One equation that lends to the universality of these results and allows for the communications BER performance presentation format is

$$\frac{E_b}{N_0} = \frac{S}{N} \cdot PG$$

in which E_b/N_0 is the SNR per bit and S/N is the signal-to-noise power ratio. When $PG = 1(0\text{dB})$, the communications system is not “spread” and $S/N = E_b/N_0$. This situation corresponds to the rightmost curve in each communications performance plot. This relationship is clearly evident when comparing the lines superimposed on Figures B1 and B2.

The only detectors used in this analysis are the radiometer (wide-band energy detector) and likelihood ratio test implementations for both frequency-hopped and direct sequence spread spectrum signals. Detectors that exploit the cyclostationary properties of these waveforms were not considered because of the added complexity that would have been introduced into this study. It should be noted that the CHESS waveform can be modified just as any other frequency-hopped waveform to combat these cyclostationary detectors at the price of increased processing.

Conjectures and Verifications

- **CHESS is more energy efficient than fixed FH for same spreading factor, which implies that CHESS demonstrates better LPD/LPI than fixed FH.**

For a fixed frequency hopping system with 1 bit per hop in an AWGN channel and using non-coherent demodulation of binary FSK, the formula for the probability of error P_e is given in Table B1. In this same table is the formula for the SD CHESS union bound symbol error probability in an AWGN channel. In the analyzed case of 1 bit per symbol (equivalent to 1 bph), the SNR per symbol in the SD CHESS formulation is equivalent to the SNR per bit in the BFSK equation so that

$$\gamma = \gamma_b = \frac{E_b}{N_0} = \frac{S}{N} \cdot PG.$$

Making this substitution into both bit error probability equations allows for the creation of a family of theoretical performance curves for both modulation/demodulation approaches. These curves are shown in Figure B5 for BFSK, and in Figures B9, B10, and B11 for SD CHESS with M equal to 16, 64, and 16,384, respectively.

Upon comparing performance curves in Figures B5 and B10, it is seen that BFSK requires approximately 6 dB more signal-to-noise power ratio (SNPR) than the SD CHESS union bound with $M = 64$ to achieve bit error probabilities between 10^{-3} and 10^{-6} . This difference increases with increasing M to approximately an 8dB difference between BFSK and SD CHESS with $M = 16,384$.

Therefore, lower energy is required by CHESS than by a fixed BFSK system with the same error performance when 1 data bit is transmitted per hop. That is, CHESS is more energy efficient than fixed FH for the same spreading factor, which implies that CHESS demonstrates better potential for LPD/LPI than fixed FH.

- **CHESS and DSSS over the same BW have the same LPD/LPI characteristics when the threat is a radiometer**

To evaluate this conjecture, the LPI margin metric is used. This MOE is discussed in Appendix A and can be denoted informally in mathematical terms as

$$\text{LPI Margin} \equiv \frac{\text{Input SNR } (P_D = x)}{\text{Input SNR } (P_e = y)}.$$

It is expected that the LPI margin will be less than unity (or negative when using dB) because a waveform should be easier to detect than to demodulate.

For a BPSK DSSS system in an AWGN channel, the formula for the probability of a bit error P_e is given in Table B1. In this same table is the formula for the SD CHESS union bound symbol error probability in an AWGN channel used in the previous conjecture. The families of communications performance curves are shown in Figure B2 for BPSK DSSS, and again in Figures B9, B10, and B11 for SD CHESS with M equal to 16, 64, and 16,384, respectively.

Upon comparing performance curves in Figures B2 and B10, it is seen that BPSK DSSS requires between 1.5 and 2.5 dB more SNPR than the SD CHESS union bound with $M = 64$ to achieve bit error probabilities between 10^{-3} and 10^{-6} . This difference increases with increasing M to the 3.5 to 4.5 dB range between BPSK DSSS and SD CHESS with $M = 16,384$. The BPSK DSSS

performance is marginally better when the bit error probability is on the order of 10^{-1} but this is an unacceptable operating regime.

The wide-band energy detector or radiometer is the most elementary and easy to implement detector. The processing block diagram for the radiometer is shown in Figure 1. A single performance equation is given for the radiometer in Table C1 with some corresponding performance curves in Figures C1 through C4. The reason for this single equation is that, for large time-bandwidth product ($TW > 1000$) signals in AWGN, its performance is the same for all frequency hopped and direct sequence spread spectrum waveforms.

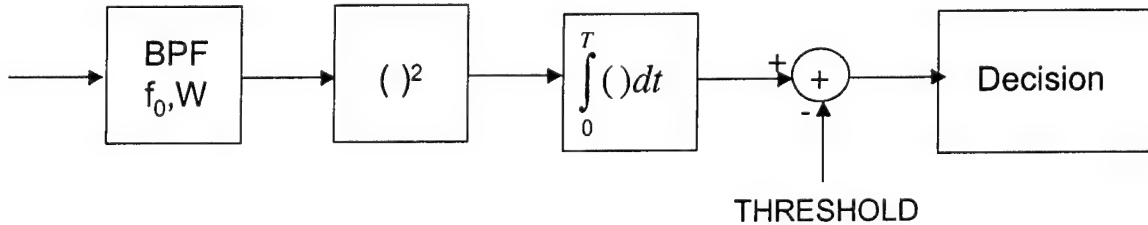


Figure 1. Radiometer Processing Block Diagram

Therefore, any differences in the LPI margin between BPSK DSSS and SD CHESS result from differences in the communications performance. Then, based on the discussion above, SD CHESS is slightly more energy efficient than BPSK DSSS (between 1.5 and 4.5 dB) over the same BW so that it has similar or better LPD/LPI characteristics when the threat is a radiometer. An example value for the LPI margin for SD CHESS ($M = 64$) can be taken from Figures B10 and C2. With $PG = 27$ dB, $P_e = P_{fa} = 10^{-6}$, $TW = 10^6$, and $P_D = 0.9$, the theoretical LPI margin is approximately $-22\text{dB} - (-18\text{dB}) = -4\text{dB}$.

An additional result identified in this study is that SD CHESS has better LPD/LPI characteristics than BPSK DSSS over the same bandwidth when the threat is an optimum detector in that it implements a likelihood ratio test (LRT). The LRT detector for frequency hopped waveforms is termed the optimum multichannel FH pulse matched ED and its processing block diagram is shown in Figure 2. The performance equation is given in Table C1 with some corresponding performance curves in Figures C5 through C8. This equation holds when the waveform contains greater than 100 hops and the individual hop time bandwidth product is unity.

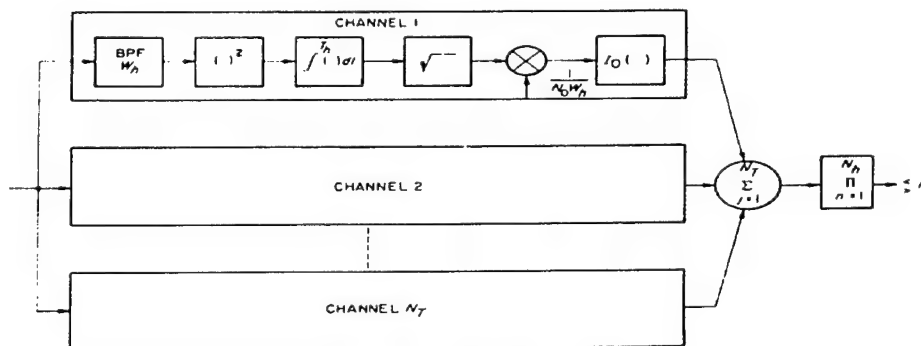


Figure 2. Optimum Multichannel FH Pulse Matched ED Processing Block Diagram

The LRT detector for DSSS waveforms is termed the synchronous coherent detector. The assumption behind this detector is that the signal phase is known to the interceptor. The performance equation is given in Table C1 with some corresponding performance curves in Figures C9 through C12.

Because the performance of these two LRT detectors differs, the LPI margin for BPSK DSSS and SD CHESS ($M = 64$) needs to be calculated using Figures B2, B10, and C4 through C12. An example set of LPI margins is shown in Table 1. The calculated values for SD CHESS ($M = 64$) are on the order of 4.5 dB higher than the corresponding values for BPSK DSSS. So, CHESS exhibits better LPD/LPI potential.

LPI Margin, dB ($PG = 27$, $TW = 10^6$, $N_T = 400$)					
LRT Detector		SD CHESS		DSSS	
		$P_e = 10^{-3}$	$P_e = 10^{-6}$	$P_e = 10^{-3}$	$P_e = 10^{-6}$
$P_{fa} = 10^{-3}$	$P_d = 0.9$	-2.5	-5.4	-6.3	-10.0
	$P_d = 0.1$	-5.7	-8.6	-10.2	-13.9
$P_{fa} = 10^{-6}$	$P_d = 0.9$	-1.8	-4.7	-4.8	-9.5
	$P_d = 0.1$	-3.3	-6.2	-7.5	-11.2

Table 1. Likelihood Ratio Test Detectors LPI Margin Example

- CHESS and DSSS have similar AJ performance for WB jammers

The model used for wide-band jamming in this analysis assumes a spectrally-flat barrage jammer across the entire communications bandwidth. In this case, the total jammer power can be calculated as $J = J_0 W$ in which J_0 is the jammer PSD and W is the signaling bandwidth.

For a BPSK DSSS system in the presence of this form of WB jamming, it can be shown [3] that the error probability is

$$P_e = \frac{1}{2} \operatorname{erfc} \left(\sqrt{\frac{E_b}{J_0 I(\alpha)}} \right) = \frac{1}{2} \operatorname{erfc} \left(\sqrt{\frac{S}{J I(\alpha)} PG} \right)$$

as given in Table B1 where

$$I(\alpha) = 2 \int_0^{\alpha} \left(1 - \frac{x}{\alpha}\right) \frac{\sin \pi x}{\pi x} dx$$

and $\alpha \equiv WT_c$. The assumptions used in this study yield $\alpha \approx 1$ and $I(\alpha) \approx 3/4$. This approximate value is taken from Figure B3.

It is normally assumed that the jammer PSD is considerably stronger than the noise PSD, e.g. greater than 10dB. In this case, the SD CHESS union bound symbol error probability in an AWGN channel can be used with the modification that $S/N \rightarrow S/(N+J) \approx S/J$. Making this substitution allows for the creation of a family of theoretical performance curves for both modulation/demodulation approaches. These curves are shown in Figure B4 for BPSK DSSS, and in Figures B9, B10, and B11 for SD CHESS with M equal to 16, 64, and 16,384, respectively.

Upon comparing performance curves in Figures B5 and B10, it is seen that BPSK DSSS requires only approximately 0.4 dB more SNPR than the SD CHESS union bound with $M = 64$ to achieve a bit error probability of 10^{-3} and approximately 1.3 dB more SNRP to achieve $P_e = 10^{-6}$. This difference increases with increasing M to approximately 2.4 and 3.3 dB for SD CHESS with $M =$

16,384. . The BPSK DSSS performance is marginally better when the bit error probability is on the order of 10^{-1} but this is an unacceptable operating regime.

Therefore, a little less energy is required by CHESS than by BPSK DSSS with the same error performance in the presence of WB jamming. This demonstrates that CHESS and DSSS have similar anti-jam performance for WB jammers.

- **CHESS has better LPD/LPI characteristics than DSSS over the same BW in a Rayleigh-fading channel**

The Rayleigh fading channel is a more appropriate model for signals that propagate with multipath and fading. With this model, the received signal $r(t)$ is of the form

$$r(t) = \alpha e^{-j\phi} s(t) + w(t)$$

in which the amplitude α is a Gaussian distributed random variable, the phase ϕ is a uniformly distributed random variable, $s(t)$ is the transmitted signal, and $w(t)$ is AWGN. In this case, the expected SNR per bit is used and is calculated as

$$\bar{\gamma}_b = \frac{E_b}{N_0} \cdot E\{\alpha^2\} = \frac{S}{N} \cdot PG \cdot E\{\alpha^2\}.$$

It is well known that diversity at the receiver can be used in Rayleigh fading channels to gain back as much as possible of the communications performance loss relative to that of the AWGN. The CHESS waveform has built in diversity due to the DFH modulation.

For a BPSK DSSS system in a Rayleigh fading channel, the formula for the probability of a bit error P_e is given in Table B1. In this same table is the formula for the SD CHESS union bound symbol error probability in a Rayleigh fading channel. In the analyzed case of 1 bit per symbol (equivalent to 1 bph), the SNR per symbol in the SD CHESS formulation is equivalent to the average SNR per bit in the BPSK DSSS based on the previous equation with $\bar{\gamma} = \bar{\gamma}_b$. Making this substitution allows for the creation of a family of theoretical performance curves for both modulation/demodulation approaches. These curves are shown in Figure B12 for BPSK DSSS, and in Figures B17, B18, B19, and B20 for SD CHESS with M equal to 16, 64, 1024, and 16,384, respectively.

Upon comparing performance curves in Figures B12 and B17, it is seen that BPSK DSSS requires approximately 13 dB more SNRP than the SD CHESS union bound with M = 16 to achieve a bit error probability of 10^{-3} and approximately 21 dB more SNRP to achieve $P_e = 10^{-4}$. This difference increases with increasing M to approximately 17 and 24 dB for SD CHESS with M = 64, and to approximately 19 and 27 dB for M = 16,384.

Therefore, lower energy is required by CHESS than by a BPSK DSSS system with the same error performance. Assuming that the detector performance is identical for both waveforms implies that CHESS demonstrates significantly better potential for LPD/LPI than BPSK DSSS in a Rayleigh fading channel.

- **CHESS performs better than DSSS in presence of repeat jammers**

If a narrow-band repeat jammer follows quickly enough to transmit at the CHESS frequency during the hop dwell time, the received energy at the receiver will actually increase, which increases the detection capabilities of the intended receiver instead of blocking the reception of the tone. Even if the jammer is slow enough that it tries to jam the transmission frequency for a

previous interval, a RAKE filter can be used at the CHESSE receiver to harvest the energy of the jamming signal and increase the detection capabilities. That is, the jamming signal will appear as a strong multipath signal that has been recovered by the RAKE receiver. If a RAKE filter is not used for the delayed jamming case, the jamming signal can either be considered a false "hit" by the receiver or can be considered a repetition of the message.

Using informal mathematical notation, the above can be expressed as follows. In the absence of a repeat jammer, the CHESSE bit error probability is a function of the SNR per bit so that

$$P_e = f(E_b / N_0).$$

Remember that the bit error probability decreases with increasing SNR per bit. If the jammer repeats with no lag from the CHESSE signal, then the SNR per bit is increased by the jammer power spectral density, which has the effect of reducing the bit error probability and can be shown mathematically as

$$P_e = f((E_b + J_0) / N_0).$$

When the jammer lags the CHESSE system by a percentage α of the dwell time, then the performance becomes

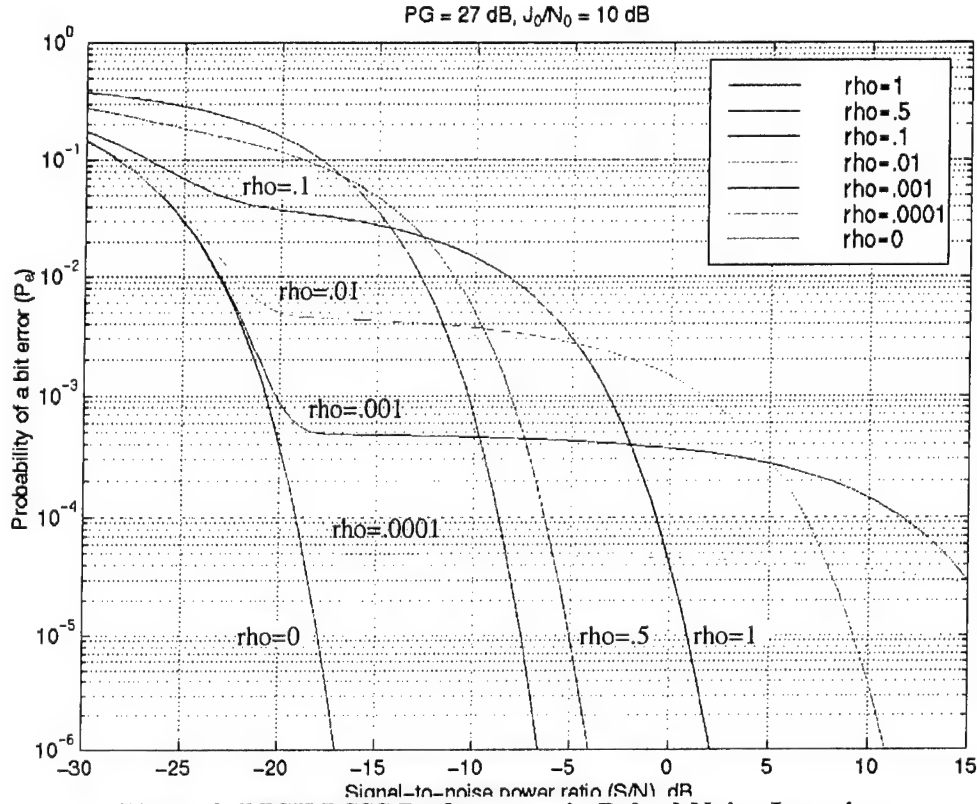
$$P_e = \begin{cases} f([E_b + (1-\alpha)J_0] / N_0), & \alpha < 1 \\ \max\{f(E_b / N_0), f(J_0 / N_0)\}, & \alpha > 1 \end{cases}$$

Making the reasonable assumption that $J_0 \gg E_b$, then, based on this simple analysis, the worst CHESSE performance in the presence of a repeat jammer is equal to the CHESSE performance when no jammer is present.

For a BPSK DSSS system, the jamming signal will be included in the received signal after it is de-spread by the receiver, thus corrupting information. This degradation in performance can be analyzed using the case of a pulsed noise jammer that is on for a percentage ρ of the time. While this assumption does not exactly match the repeat jammer case, it can easily be argued that the pulsed noise jammer is conceptually close to a repeated signal with corruption, e.g. phase, amplitude. The bit error probability equation for BPSK in the presence of a pulsed noise jammer is approximately

$$\bar{P}_e \cong (1-\rho)Q\left(\sqrt{\frac{2E_b}{I(\alpha)N_0}}\right) + \rho Q\left(\sqrt{\frac{2E_b}{I(\alpha)(N_0 + J_0/\rho)}}\right).$$

This equation is plotted in Figure 3 for $0 \leq \rho \leq 1$, $PG = 27\text{dB}$, and $J_0/N_0 = 10\text{dB}$. BPSK DSSS performance in the presence of continuous wide-band jamming is characterized by both the $\rho = 0$ and $\rho = 1$ curves. The difference between these two curves is the additional 10dB of jamming power spectral density, i.e. $J_0/N_0 = 10\text{dB}$. Therefore, the separation between these two curves will track the J_0/N_0 ratio. The remaining five curves in Figure 3 exhibit the performance characteristics induced by the "repeat" jammer. They track the $\rho = 0$ curve when the signal power is low, flatten out at approximately $P_e = \rho/2$ (i.e. random guesses during the jamming which in a sense occurs every $1/\rho$ bits) for transitional values of the signal power, and then fall off with high-amplitude signals. So for example, at an operating point of $P_e = 10^{-4}$, BPSK DSSS in the presence of a repeat jammer can require as little as 0.5dB more SNR ($\rho = .0001$) or as much as 30dB more SNR ($\rho = .001$) over the same signal in the absence of a repeat jammer.



- Even though CHES is less energy efficient than TCM, it occupies significantly greater bandwidth, so the overall LPD/LPI performance of CHES is better.

To examine the trellis coded modulation (TCM) bit error performance as a function of SNR, we first considered the bit error expression for an M-ary QAM system, given by [3]

$$P_e = \frac{2^{k-1}}{2^k - 1} \left[1 - \left(1 - P_{\sqrt{M}} \right)^2 \right]$$

$$P_{\sqrt{M}} = 2(1 - 1/\sqrt{M}) Q\left(\sqrt{3/(M-1)} \bar{\gamma}\right)$$

$$k = \log_2 M$$

We then recall that the coding gains in going from QAM to TCM range from 3.6-5.7 dB [3], and assume a gain of 4 dB for the system under comparison. The plot of the resulting curve for M=64 is shown in Figure 4, along with the previously calculated bounds for CHES. Comparing the curves, we can see that K-ary CHES (the original hardware implementation) is *less* energy efficient than TCM, but soft-decision CHES (current simulation) is *more* energy efficient than TCM.

It is assumed that a sub-optimal implementation will produce a curve between the K-ary and soft-decision CHES curves, indicating that a sub-optimally implemented system will have energy efficiency similar to that of TCM. Given the nature of the two approaches, it is immediately

obvious that the bandwidth of CHES is wider than the bandwidth of TCM, leading us to the conclusion that the overall LPD/LPI performance of CHES is better than TCM.

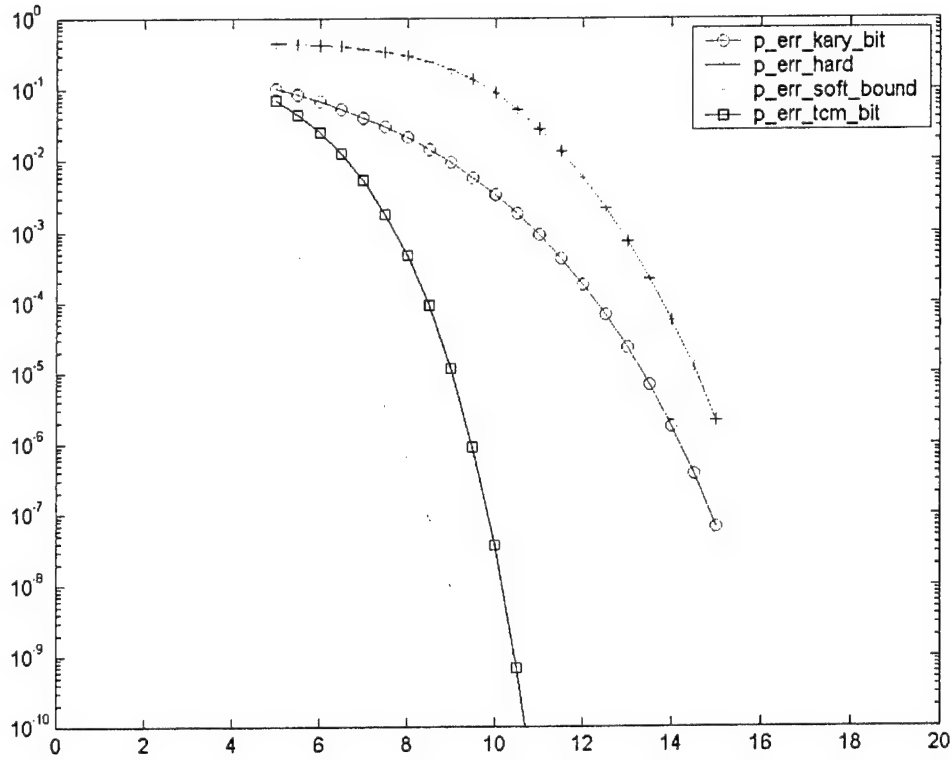


Figure 4. Comparison of CHES and TCM Energy Efficiencies

- **CHES has the potential to allow conferenced users**

We determined that CHES can allow up to $M / 2^h$ conferenced users at any time, without the additional imposition TDMA or power control. The conferencing allowed is a multipoint-to-multipoint, with the only requirements being that each conferenced user know the underlying trellis for the other users in the conference and that each conferenced user possess the processing capability to follow multiple trellisses. Each conferenced user must have a different trellis.

To verify that $M / 2^h$ conferenced users are possible, consider a stage in the trellis in which all states are possible valid transmissions.. This is the maximally occupied situation. Each occupied state represents a unique user. At the previous stage, each occupied state contains only one unique user. Because each state has 2^h branches from it, $M/2^h$ is the maximum number of users allowed to have this configuration.

It is expected that if conferencing is permitted, the missed-hop performance will degrade. It is hypothesized that if conferencing is allowed, the number of missed consecutive hops that are guaranteed to be correctable is $(\log_2 M/h)/N_c$, in which N_c is the number of conferenced users,. Other unique "signatures" associated with each user (besides their unique trellisses) can be used to increase resolvability, thereby regaining possible losses in missed hopped corrections.

A plot showing the maximum number of conferenced users as a function of bits-per-hop (h) and parameterized by hop set size (M) is shown in Figure 5.

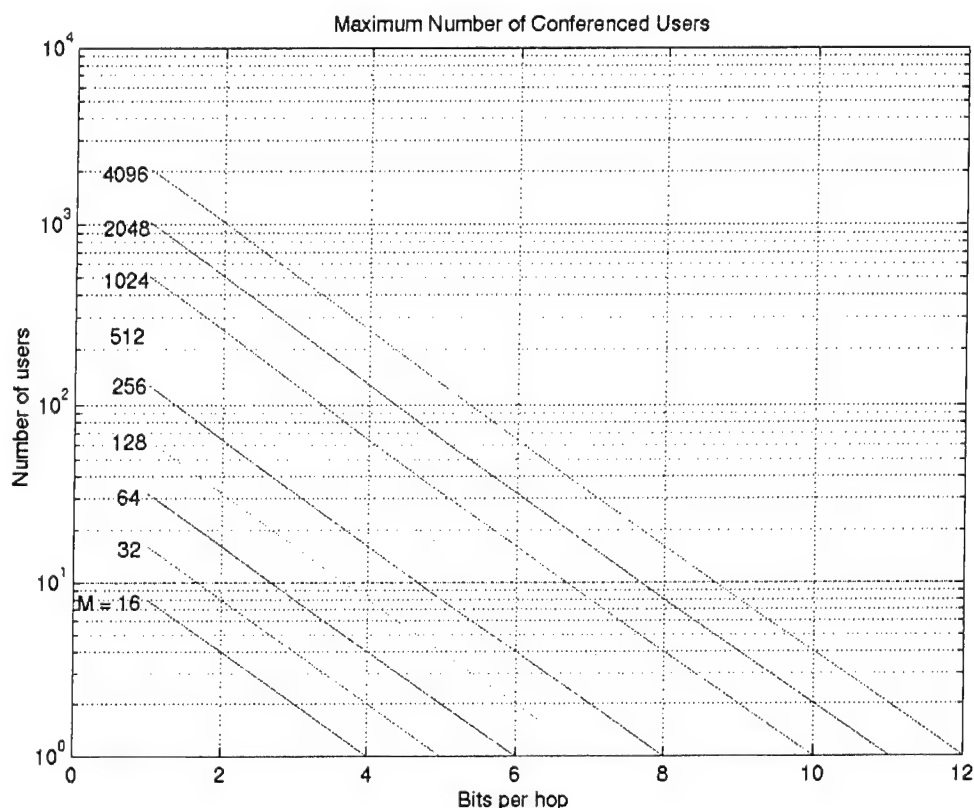


Figure 5. Maximum Number of CHES Confereed Users

- A better hop-pattern choice will improve the BER of CHES by improving the error-correcting capability of the trellis (i.e. increasing the number of misses and false hits that can be corrected), thereby also improving the energy efficiency and AJ performance.

The capability to correctly determine missed hops is an important feature of CHES. With this capability, CHES is able to provide the user with burst error correction capability with no loss in information rate and resistance to narrow-band jamming.

First, it was determined that the number of correctable consecutive missed hops is $\text{floor}(\log_2(M)/h) - 1$. To understand this, consider a CHES trellis in which the last transmitted state was correctly received. At that point, there are $K = 2^h$ possible paths from the last known state, and each path is distinct. After 2 hops, there are 2^{2h} paths, all distinct. Continuing on, the maximum number of possible distinct paths is M , reached after $\log_2 M/h$ steps. If the $\log_2 M/h$ -th state is not known, the paths interleave and it is not possible to correct the missed hops. Therefore up to $\log_2 M/h - 1$ hops can be lost and subsequently corrected.

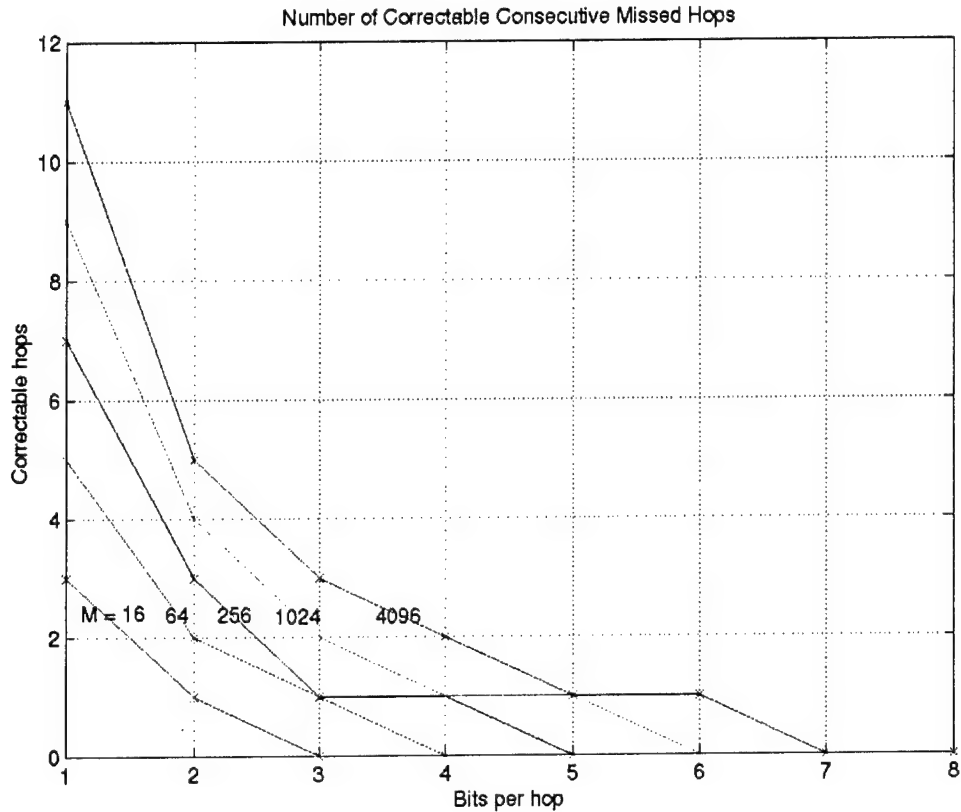


Figure 6. Number of Correctable Consecutive CHES Missed Hops

Figure 6 shows the number of correctable consecutive missed hops as a function of h and M . An example showing the trellis for a hop set size of 8 and one bit per hop is shown in Figure 7. Two consecutive hops are missed, but the trellis structure allows the receiver to determine what the missing transmissions were.

A standard notation for rate k/n convolutional codes is (n, k, m) , where the number of shift registers on each of the k input lines is m_i , $i=1$ to k , and the memory order $m = \max(m_i)$. The number of states in the associated trellis is then $2^{\sum m_i}$. Only CHES systems which encode one bit per hop (i.e. $k=1$) are considered in this preliminary analysis. The analysis will be extended to $k>1$ at a future date. The current CHES system has a hop pattern that may be modeled by a shift-register $(\log_2(M), 1, \log_2(M))$ convolutional code with the n -bit output associated with each transition each to the state on which the transition terminates at the next stage. For example, the trellis associated with the $(3, 1, 3)$ CHES hop pattern is shown in Figure 8. It has $M=8$ states. Examining the trellis, it can be seen that the free distance is 3. For a general $(\log_2(M), 1, \log_2(M))$ CHES hop pattern (with the shift register-based hop pattern) the free distance will be $\log_2(M)$, the number of shifts that are required to clear the first deviation from the all-zero path. From the free distance, we can approximate the bit error probability for soft decoding using an upper bound on the first error event probability.

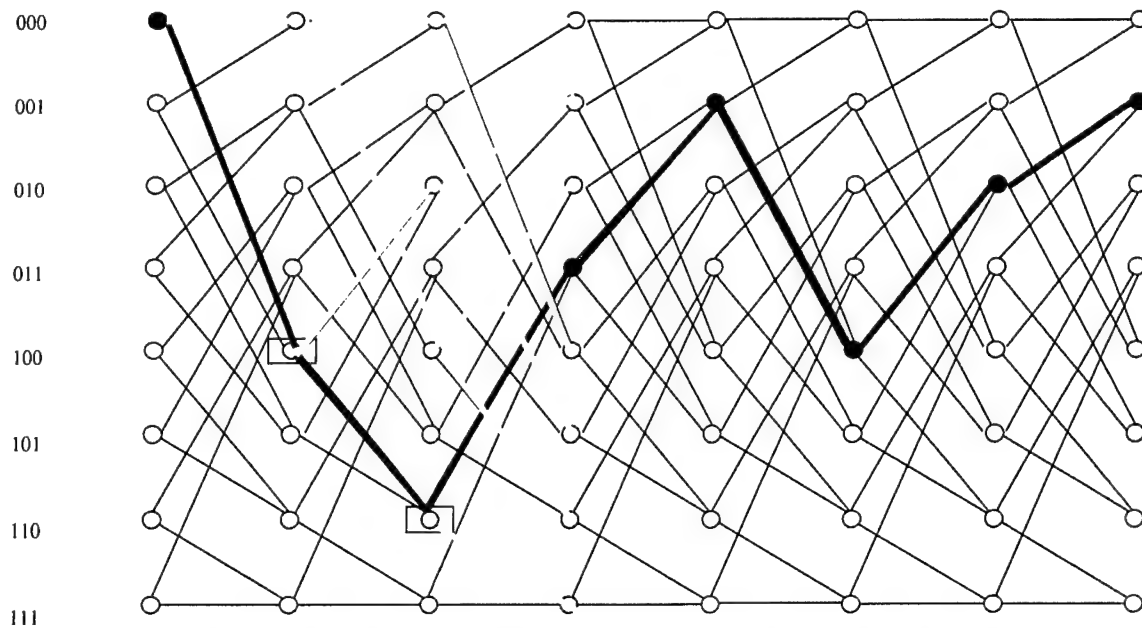


Figure 7. Missed Hop Correction Example for Hop Set Size of 8 and One BPH

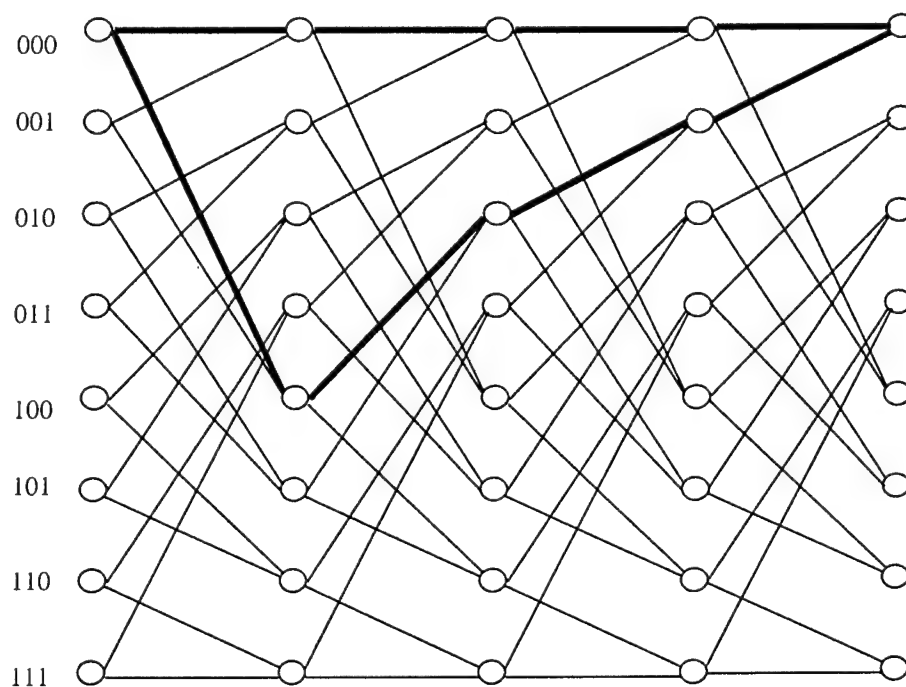


Figure 8. Convolutional Code Trellis with Error Path

An approximate upper bound on the error probability for a convolutional code with free distance d_{free} is [3,4]

$$\tilde{P}_{ub} = (1/2) \sum_{d=d_{\text{free}}}^{\infty} a_d * X^d \Big|_{X=\exp(-R_c E_b / N_0)}$$

in which a_d is the number of codewords of weight d . Preliminary work indicates that the above equation can be simplified for the shift-register hopping pattern of the CHESS system, but the work remains to be verified. Even from the general equation presented above, it can be seen that the first term is the dominating term, indicating the importance of d_{free} as a performance parameter.

As a concrete example of a case for which a better hopping pattern is available, consider the rate $\frac{1}{2}$ convolutional code with 4 state, 2 shift-register, [4] lists the encoding matrices for the $(M, 1, \log_2(M))$ codes with the following free distances. The free distances from [4] are compared to the CHESS shift-register free distances in Table 2.

M	Log2(M)	d_{free} (CHESS)	d_{free} (achieved with other codes)
4	2	2	5
8	3	3	10
16	4	4	16

Table 2. Free Distance Comparison Between CHESS and the $(M, 1, \log_2(M))$ Codes

The increase from a free distance of 4 for the 16 state $(4, 1, 4)$ shift-register encoder and a free distance of 16 for the optimal $(4, 1, 4)$ encoder results in significantly improved error performance. For larger M , we can use the Plotkin bound ($d_{\text{free}} \leq (n(n+h)/2) * 2^{hk} / (2^{hk} - 1)$), $h=1, 2, \dots$ for a rate k/n code) to give an upper bound on d_{free} . (Note: The Plotkin bound loosens as n increases. It is likely that tighter bounds are published in the literature.) The values for the Plotkin bound are compared to the free distance for shift-register CHESS in Table 3.

M	Log2(M)	d_{free} (CHESS)	d_{free} (Plotkin bound)
4	2	2	5
8	3	3	10
16	4	4	16
32	5	5	22
64	6	6	30
128	7	7	40

Table 3. Free Distance Comparison Between CHESS and the Plotkin Bound

The larger values for the free distance indicate that significant gains can be made by carefully choosing a hopping pattern. It should be remembered that the above values for d_{plotkin} are *upper* bounds on the free distance, and that the bounds loosen as n increases. Even if the bounds are loose, the bounds (for larger values of M) and the codes that achieve optimal distance (for lower values of M) indicate that significant improvement in error performance, and therefore in missed and false hop correction, can be achieved with a different choice of trellis structure. Note that if a hopping pattern is chosen based on a more powerful convolutional code with the same rate and memory order, the decoding of the improved trellis has not gained in complexity. The exact codes that achieve or approach the upper bounds must still be found. It is expected that the optimal codes for rate $1/n$ codes with larger values of n have been tabulated in the literature, but a source has not yet been identified. Note that if a hopping pattern is chosen based on a more powerful convolutional code with the same rate and memory order, the decoding of the improved trellis has not gained in complexity.

- **CHESS has better AJ performance than DSSS for NB jammers**

The correctable missed hop feature of CHESS detailed in the previous conjecture and summarized by Figure 6 provides excellent resistance to narrow-band (NB) jamming by offering a burst error correction capability with no loss in the information rate. Based on this feature, it can be assumed that a narrow-band (NB) jammer has little to no effect on CHESS waveform performance.

In the presence of NB jamming, the equation in Table B1 for DSSS in AWGN still holds if the ratio E_b/N_0 is replaced with $E_b/(N_0 + J_0)$. It is normally assumed that the jammer PSD is considerably stronger than the noise PSD, e.g. greater than 10dB. Therefore, BPSK DSSS in the presence of NB jamming requires $[J_0/N_0]$ dB more SNR to achieve the equivalent performance of BPSK DSSS in the absence of NB jamming.

To compare the AJ performance of CHESS and BPSK DSSS, consider the black vertical lines in Figures 9 and 10. These lines indicate the intersection of the $PG = 18$ dB curves with the $P_e = 10^{-3}$ line for BPSK DSSS plus a 10dB NB jammer (at $SNRP \approx -2$ dB) and for SD-CHESS with $M = 64$ (at $SNRP \approx -13$ dB), respectively. So, in this example BPSK DSSS requires approximately 11dB more SNRP to achieve the equivalent performance of CHESS.

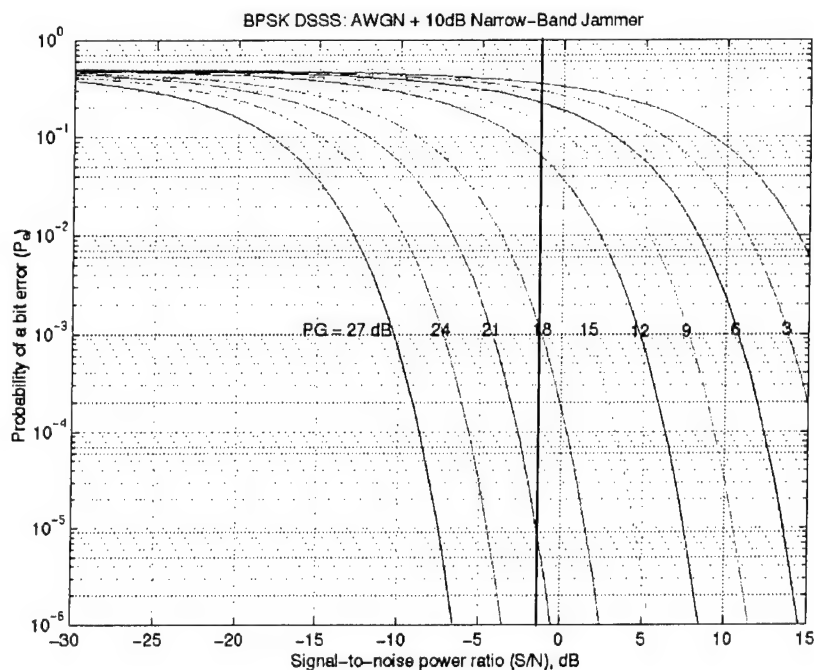


Figure 9. BPSK DSSS Performance in AWGN with a 10dB NB Jammer

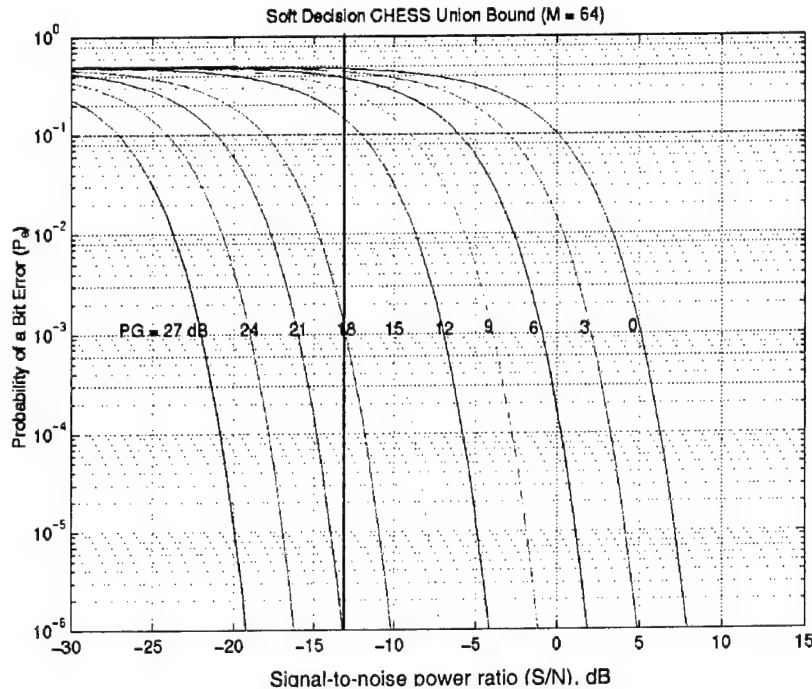


Figure 10. SD CHES (M = 64) Performance in AWGN

- CHES has potential for self-synchronization (vs pilot tone synch for DSSS, and synch for fixed FH)

The potential for self-synchronization is a result of the trellis structure of CHES and its ability to correct missed hops. A self-synchronizing system is less likely to be detected by an interceptor because the cyclic synch sequence is not required. DSSS requires a pilot tone and fixed FH requires periodic synch sequences. The CHES systems uses the actual transmitted data (not a synch sequence) and the trellis nature of the waveform to converge to the correct path on the trellis. Based on rules-of-thumb for the convergence of convolutional codes using Viterbi decoding, the CHES system could require up to $10 \cdot \log_2(M)$ transmission intervals before converging to the correct path. However, if the information is stored, once the decoder has converged, it can go back to the ambiguous portion of the trellis and use the missed-hop correction capabilities to "fill-in" portions of the sequence. It should be noted that systems that rely on synch sequences lose the opportunity to transmit information bits during the synch intervals.

- Practical implementation of CHES is easier than DSSS

Several characteristics of the CHES waveform indicate that practical implementation of CHES should be less costly than that of DSSS. For instance, CHES has a (much) smaller instantaneous bandwidth when compared to DSSS with same spreading factor. The smaller instantaneous bandwidth allows the designer to specify a retuneable, narrower BW antenna for CHES (and other single-tone FH waveforms); DSSS would require an antenna with a "wide-enough" BW. Typical instantaneous bandwidth for a tactical antenna is 5-10% of frequency band center, e.g. at 4 MHz, IBW~40 kHz, which are numbers that work easily with CHES and other FH waveforms.

A narrower instantaneous bandwidth is also desirable when considering A/D converters (ADCs). For CHESS and other FH waveforms, several ADCs for the narrower bands are less expensive than a single ADC with wide phase coherence, as required by DSSS. The CHESS algorithm, as implemented in the simulation, consists mainly of FFTs and Viterbi decoding, lending itself to straightforward FPGA implementation. Additionally, multiple trellisses for conferenced systems could then be modularly implemented. The computational complexity of the algorithm as implemented increases exponentially as M and h increase due to the Viterbi decoding. The complexity results not from the different types of operations (primarily add and compares) but from the large number of them. An FPGA implementation is one way to address this issue, but might not be sufficient for extremely large values of M . If a sub-optimal decoding method is developed at a later date to reduce the computational complexity, the ease of FPGA implementation of the revised algorithm should be considered. Finally, CHESS does not require a modulated signal, which keeps the complexity and cost of circuit boards relatively low.

MATLAB Simulation Results

A MATLAB simulation of a CHESSE system as shown in Figure 11 has been implemented. The user may define the hopset size, the frequency range of the hopset, the signal-to-noise ratio, the jamming signal level, and the size of the FFT used in the receiver. The receiver currently calculates an FFT of the received signal over the entire frequency range and then performs Viterbi decoding along the allowable paths through the trellis. This allows for both hard decision (trellis length of 1) and soft decision (trellis length greater than 1) CHESSE processing. The code has been written in a modular form so that changes can be made to components with little disruption to the remaining code.

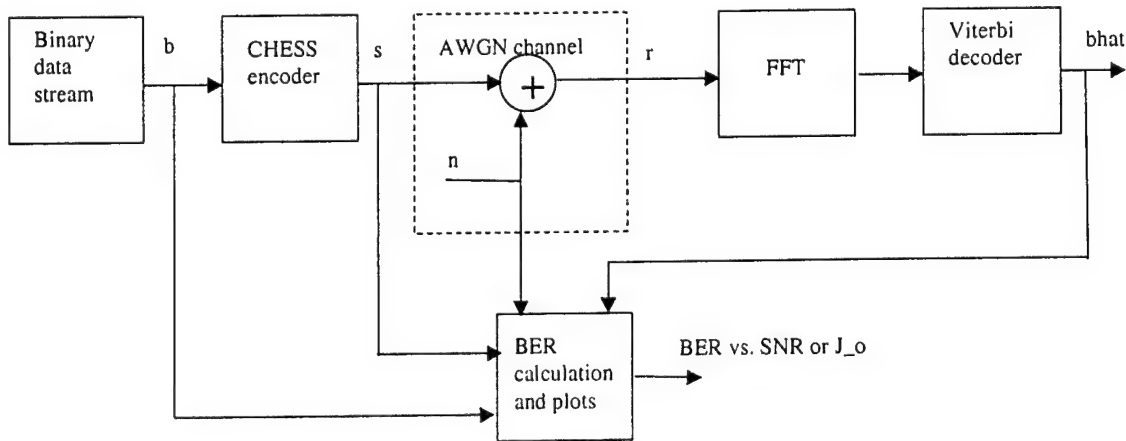


Figure 11. CHESSE Matlab Simulation Block Diagram

The simulation has been used to verify some of the basic CHESSE analysis results in an AWGN channel. Figures 12 and 13 display the results of hard decision CHESSE simulation runs relative to the corresponding theoretical curves for $M = 16$ and $M = 64$, respectively. Each plotted simulation point denotes the calculated bit error probability for 10,000 continuous message bits. The simulation results closely match the theoretical curves thereby verifying both the analysis and simulation for hard decision CHESSE.

Figures 14 and 15 display the results of soft decision CHESSE simulation runs relative to the corresponding theoretical curves for $M = 16$ and $M = 64$, respectively. The differences between the simulation results and the theoretical union bound curves show that the curves do indeed bound the performance of the Viterbi decoder and that this theoretical bound gets looser with increasing M and with increasing processing gain (PG).

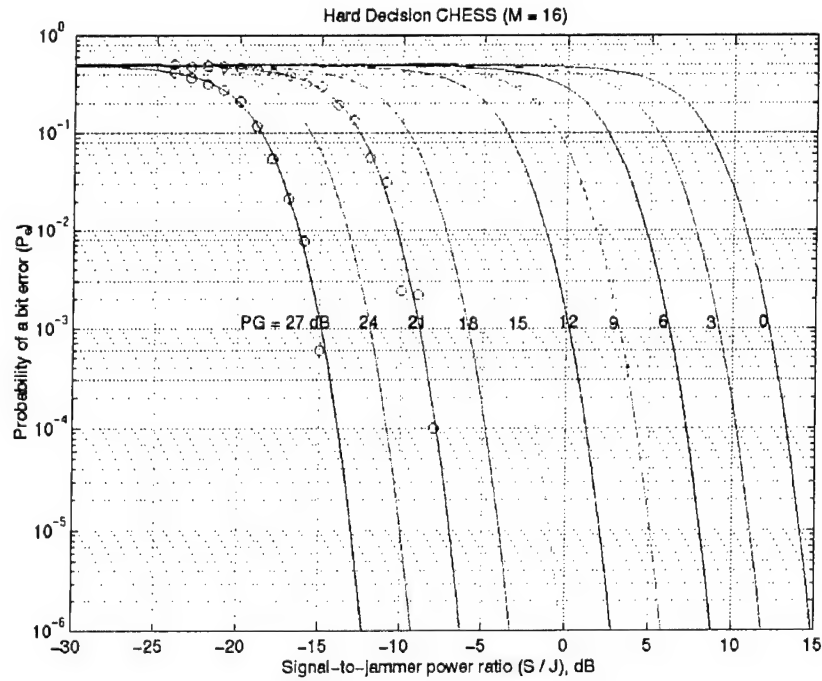


Figure 12. HD CHES (M = 16) Simulation Results

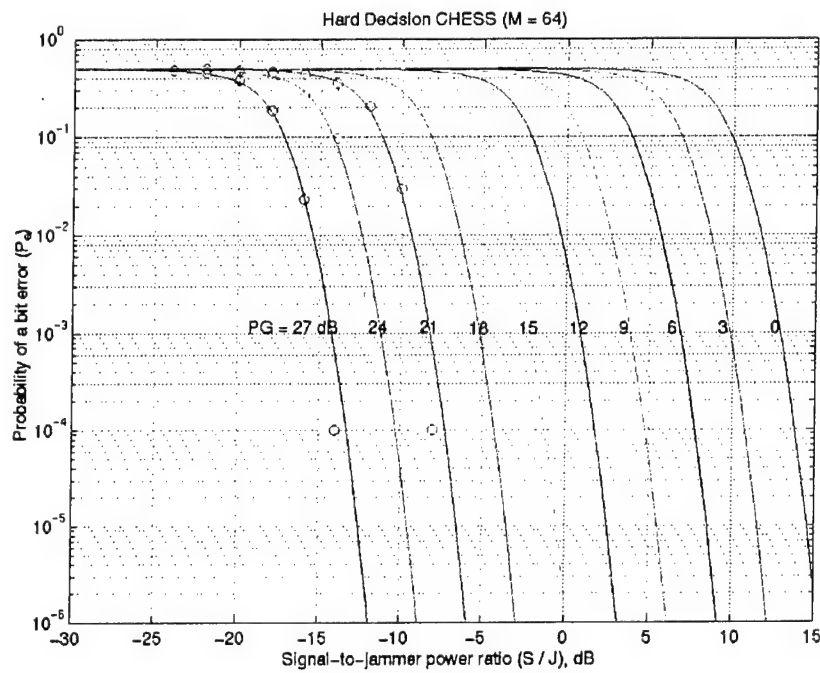


Figure 13. HD CHES (M = 64) Simulation Results

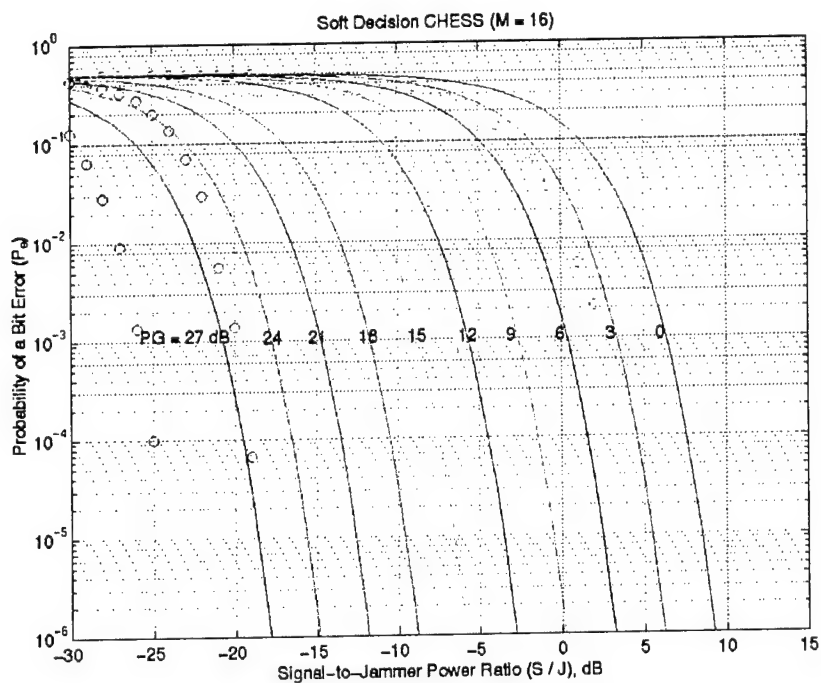


Figure 14. SD CHES (M = 16) Simulation Results
Simulation (dotted) curves correspond to PG values of 27, 21, 15, 9 and 3 dB.

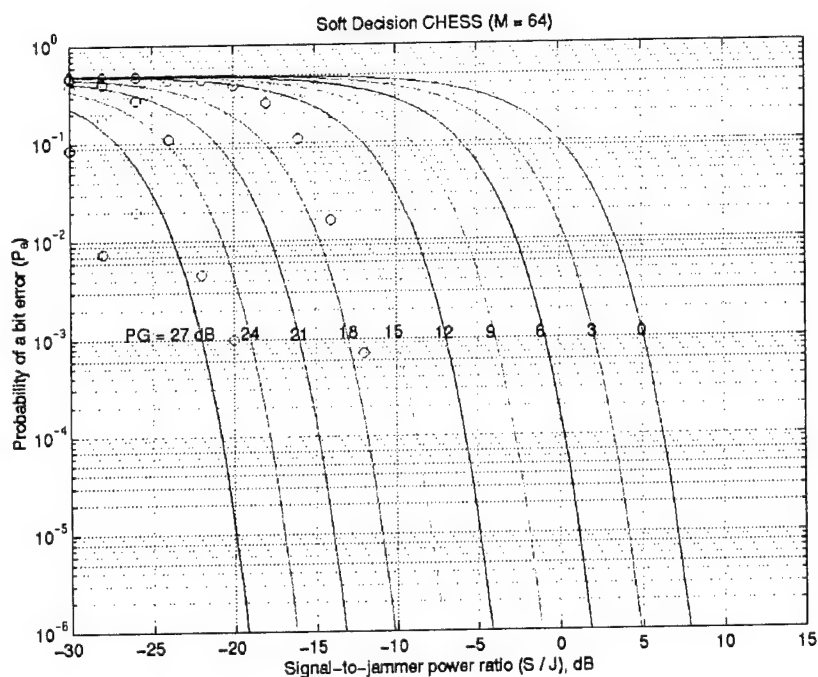


Figure 15. SD CHES (M = 64) Simulation Results.
Simulation (dotted) curves correspond to PG values of 27, 21, 15, 9 and 3 dB.

Conclusion

This study identified and quantified the advantages of CHESS and enhanced-CHESS systems in AWGN and fading channels. Performance was compared to DSSS and fixed FH systems. The basic CHESS digital radio technology exhibits many desirable performance characteristics. These are itemized below.

- *Low Probability of Detection and Intercept (LPD/LPI)*
- *Low Probability of Intercept (LPI).*
- *Anti-Jam in both AWGN and fading channels.*
- *Error Detection and Correction (EDAC).*
- *Self-synchronizing*
- *Supports conferencing*
- *Multiple bits per symbol without modulation.*
- *Insensitive to repeat jammers*

Figure 16 summarizes the results of performance comparisons between CHESS, DSSS and FH. As summarized in Figure 16, CHESS outperforms DSSS and FH under a variety of conditions, with the exception of computational complexity. For instance, the CHESS anti-jam performance in AWGN is similar to the DSSS anti-jam performance and superior to the FH anti-jam performance. Furthermore, the LPD/LPI performance of CHESS is better than DSSS and FH in both AWGN and fading channels. Compared to FH, CHESS is more tolerant of co-channel interference; CHESS is much more tolerant of co-channel interference than DSSS. When considering antenna energy efficiency, CHESS is similar to FH and 6 dB better than DSSS. Similarly, the receiver cost of both CHESS and FH are lower than the receiver cost of DSSS. It is possible to implement CHESS so that it is self-synchronizing, which neither DSSS nor FH can do. Additionally, while DSSS and FH allow conferencing when additional algorithms or protocols are overlaid on them, CHESS allows conferencing without requiring any additional infrastructure. Overall, CHESS outperforms both DSSS and FH.

CHESS Wins Performance Comparison

Feature	CHESS	DSSS	FH
Anti-Jam, AWGN Channel			
LPI/LPD Margin (fading channel)	> 19	6	0
LPD/LPI Margin (AWGN)	6	4	2
Computational Complexity			
Co-Channel Interference			
Antenna Energy Efficiency	6	0	6
Receiver Cost			
Self-synchronization			
Conferencing			

Note: -values are relative, in dB

Figure 16. CHESS outperforms DSSS and FH

To extend and exploit these results, it is suggested that analysis and implementation of CHES continue.

References

- [1] Sanders, *Proposal for CHESS Enhancement Study*, April 2000.
- [2] Sanders, CHESS Enhancement Study Kickoff Meeting, July 19,2000
- [3] Proakis and Salehi, *Communications Systems Engineering*, Prentice Hall, 1994
- [4] Lin and Costello, *Error Control Coding*

Appendix A: Performance Measures

Specific performance metrics are calculated to provide the structure for the evaluation of the conjectures in this report. The measures-of-effectiveness (MOEs) that we use are:

- Probability of a symbol error (P_e)
- Probability of detection (P_d)
- LPI margin
- Jamming margin

P_e is defined as $P(\hat{S}_k \neq S_k)$ in which $\{\hat{S}_k\}$ is an estimated symbol sequence based on the transmitted symbol sequence $\{S_k\}$. Obviously, the goal is to design for this value to be as low as possible.

P_d is a simple concept on a single transmission basis. From the viewpoint of intercept resistance, the goal is to design for this value to be as low as possible for the interceptor. However, calculating the probability that an interceptor is successful during a particular operation becomes much more complicated. Quantifying this measure requires detailed knowledge about the operational concepts for both the intercept and communications systems.

The low probability of intercept (LPI) margin measure compares the signal strength needed for a specified level of intercept success to the signal strength needed for a specified level of communications performance. An LPI communicator desires a large LPI margin so the larger this LPI margin ratio becomes, the more resistant to intercept is the communications system. We use an alternative approach and evaluate the LPI margin as the ratio of input signal-to-noise ratio (SNR) needed for intercept success to the input SNR needed for communications success. This allows for the separate evaluation of both communications (BER) and intercept (operating characteristics) performance, and for their combination into an LPI margin.

The jamming margin is defined as the ratio of jammer power to signal power that can be tolerated without reducing performance below a desired level. It can be shown that the jamming margin (for a wideband jammer) is

$$\left(\frac{P_j}{P_s} \right)_{dB} = \left(\frac{W}{R} \right)_{dB} - \left(\frac{E_b}{J_0} \right)_{dB}$$

where P_j is the power of the jamming signal, P_s is the power of the desired signal, W is the transmission bandwidth, and R is the data rate in bits per second. The quantity E_b/J_0 is the SNR per bit. This equation assumes that the jammer PSD is much greater than that of the noise. An anti-jam communicator desires a large jamming margin.

Appendix B: Communications Bit Error Performance

Bit/symbol error probability formulas

Modulation / Processing Approach	Channel	
	Additive White Gaussian Noise	Rayleigh-Fading
DSSS BPSK	$\frac{1}{2} \operatorname{erfc}\left(\sqrt{E_b / N_0}\right)$	$\frac{1}{2} \left[1 - \sqrt{\frac{\bar{\gamma}_b}{1 + \bar{\gamma}_b}} \right]$
DSSS BPSK (WB Jammer)	$\frac{1}{2} \operatorname{erfc}\left(\sqrt{\frac{E_b}{J_0 I(\alpha)}}\right)$	
BFSK	$\frac{1}{2} \exp(-E_b / 2N_0)$	$\frac{1}{2 + \bar{\gamma}_b}$
K-ary CHES	$\frac{K}{2(K-1)} \sum_{n=1}^{K-1} (-1)^{n+1} \binom{K-1}{n} \frac{1}{n+1} \exp(-n\gamma/(n+1))$	$\frac{K}{2(K-1)} \sum_{n=1}^{K-1} (-1)^{n+1} \binom{K-1}{n} \frac{1}{(n+1) + n\bar{\gamma}_b}$
M-ary CHES	$\frac{K}{2(K-1)} \sum_{n=1}^{M-1} (-1)^{n+1} \binom{M-1}{n} \frac{1}{n+1} \exp(-n\gamma/(n+1))$	$\frac{K}{2(K-1)} \sum_{n=1}^{M-1} (-1)^{n+1} \binom{M-1}{n} \frac{1}{(n+1) + n\bar{\gamma}_b}$
Hard-Decision CHES	$\delta M / (2((K-1) + (M-K)\delta)) *$	$\delta M / (2((K-1) + (M-K)\delta)) *$
Soft-Decision CHES	$\frac{K}{2^{2L}} \exp(-L\gamma/2) \sum_{n=0}^{L-1} \frac{1}{n!} \left(\sum_{k=0}^{L-1-n} \binom{2L-1}{k} \right) \left(\frac{L\gamma}{2} \right)^n$	See Proakis, <i>Digital Communications</i> , McGraw Hill, 2001 (p. 834)

Table B1. Bit/Symbol Error Probability Formulas

* δ is the appropriate K-ary CHES symbol error probability.

AWGN Channel Performance Curves

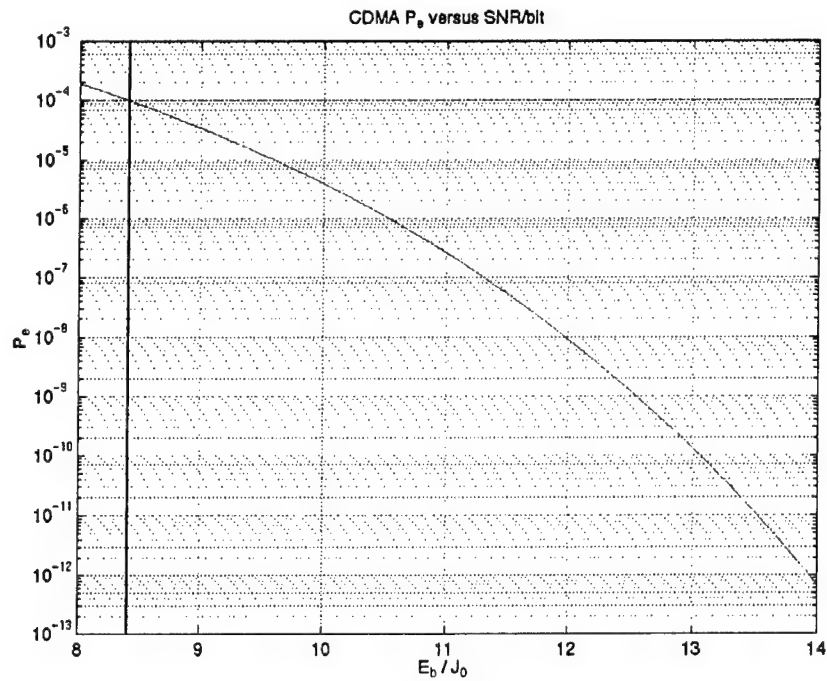


Figure B1. BPSK DSSS Performance in AWGN as a Function of SNR per Bit

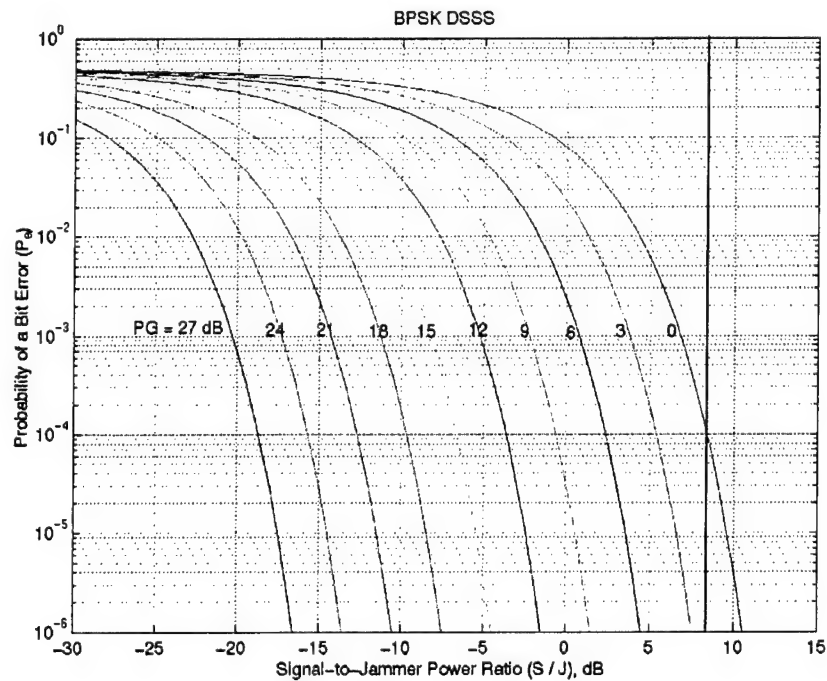


Figure B2. BPSK DSSS Performance in AWGN (also for NB Jamming)

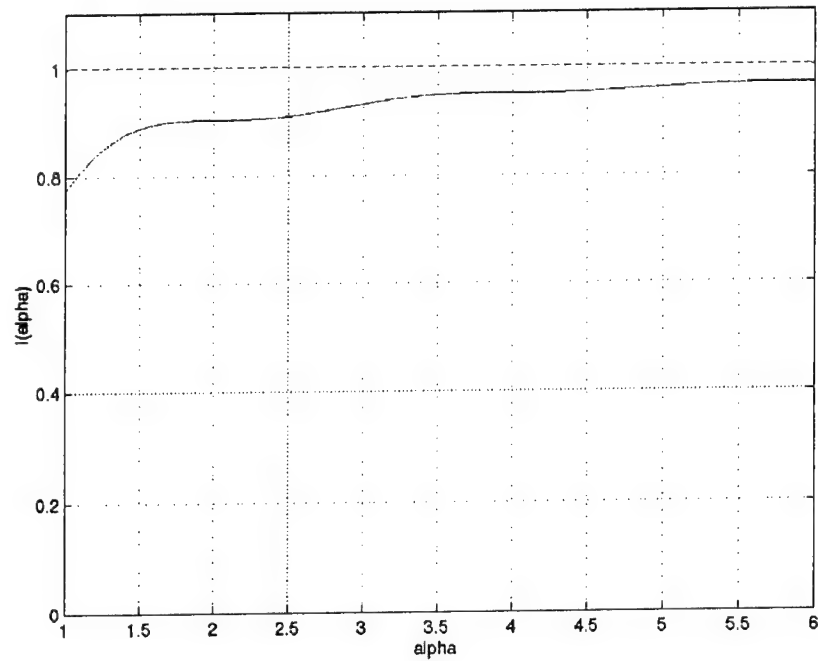


Figure B3. BPSK DSSS Wide-Band Jamming Function

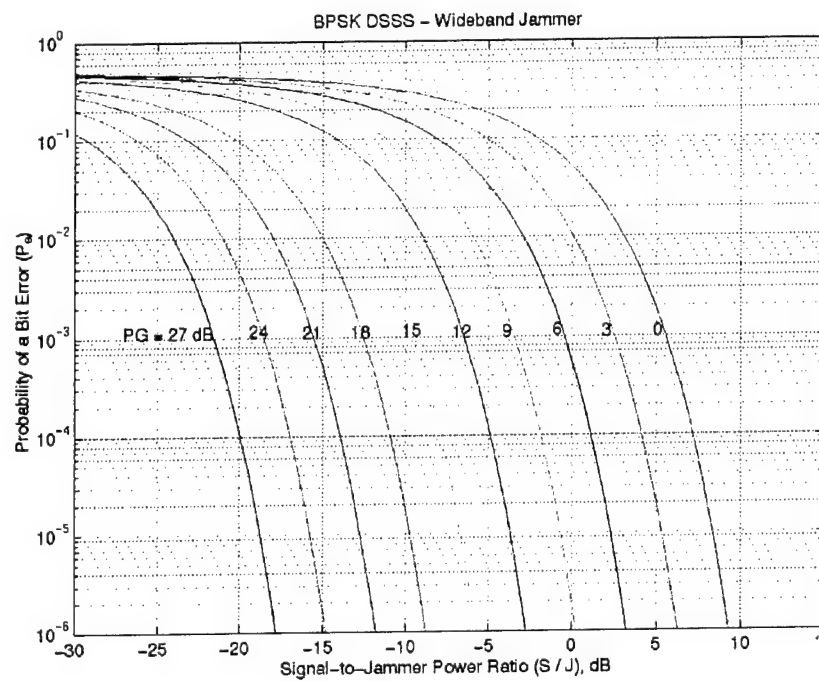


Figure B4. BPSK DSSS Performance in WB Jamming

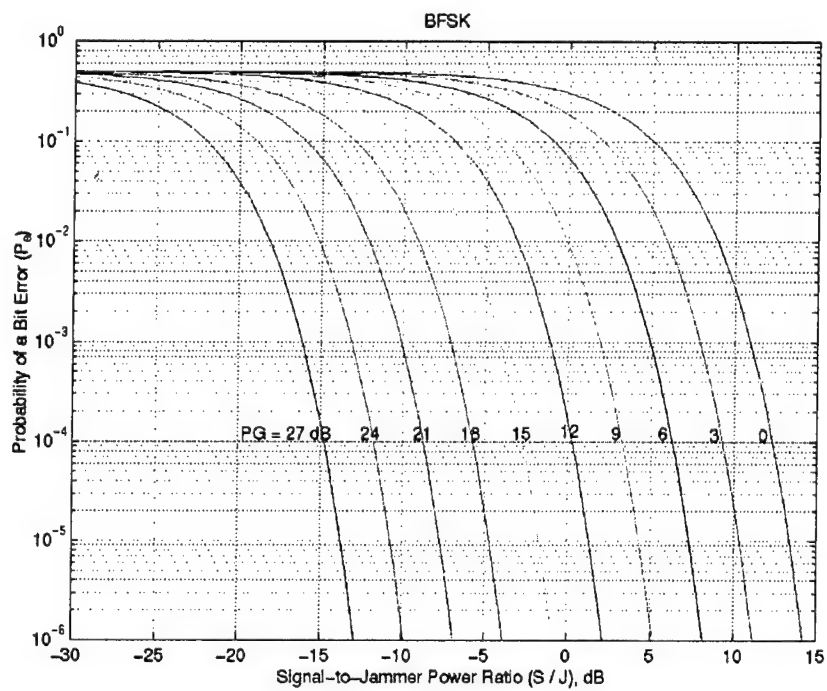


Figure B5. BFSK Performance in AWGN

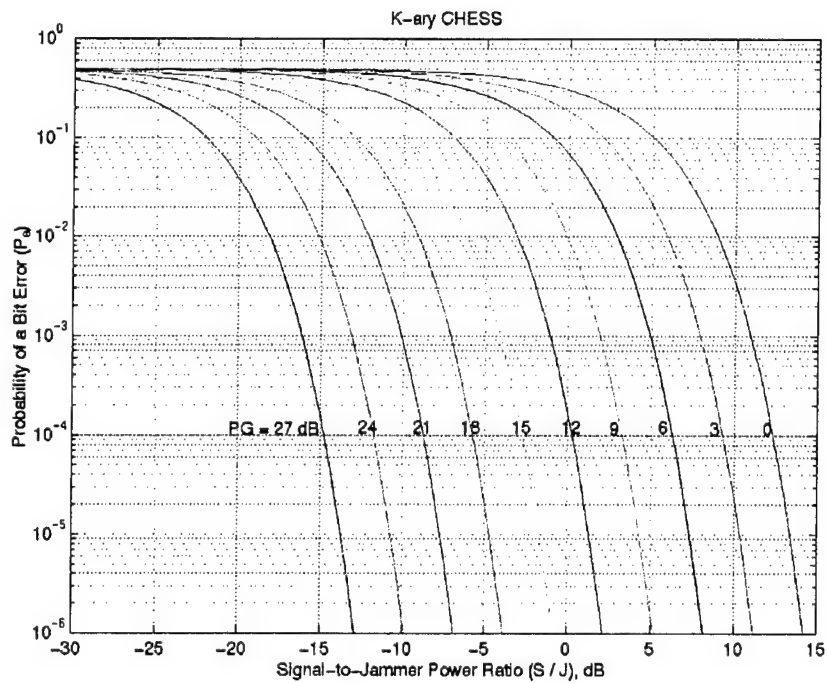


Figure B6. K-ary CHES Performance in AWGN

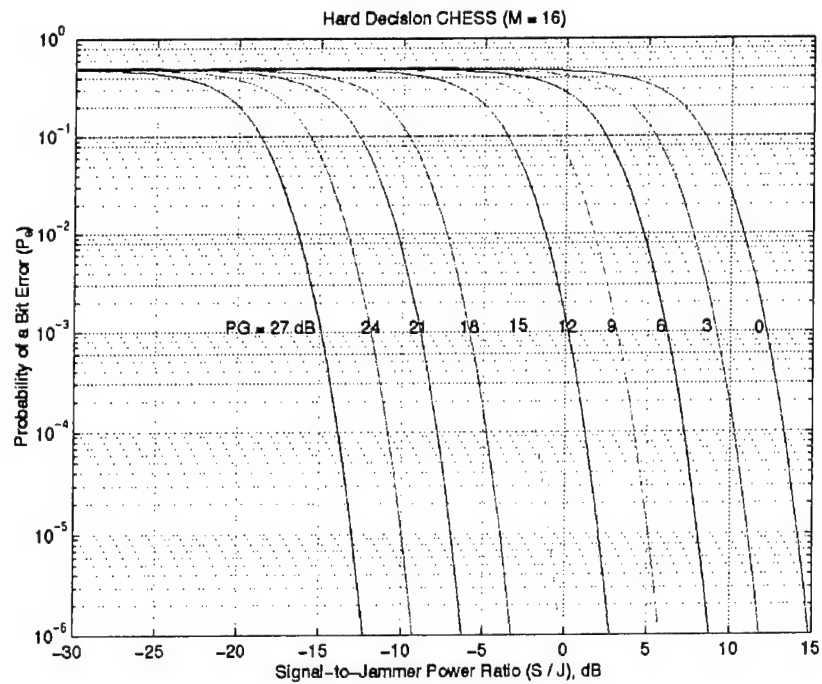


Figure B7. Hard Decision CHES (M = 16) Performance in AWGN

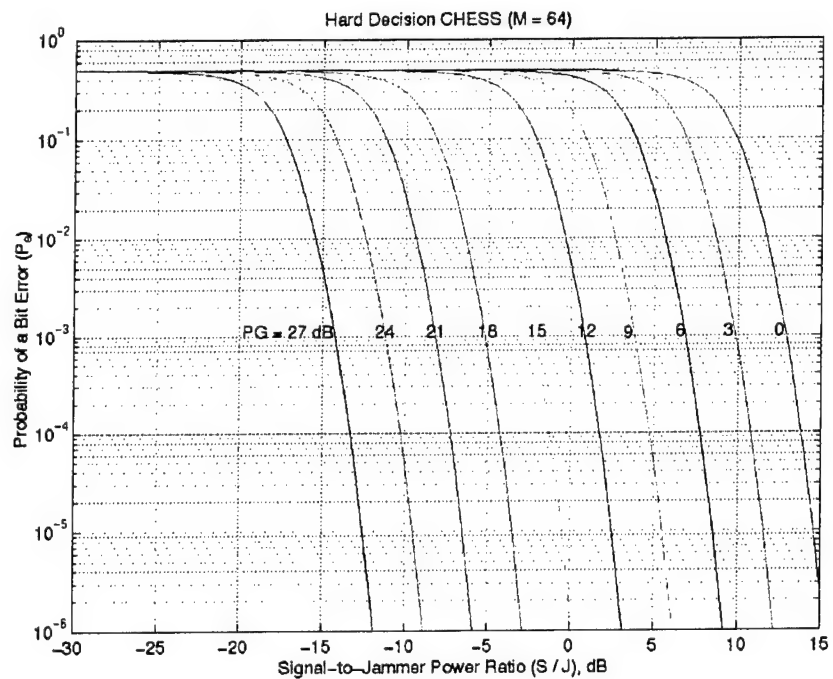


Figure B8. Hard Decision CHES (M = 64) Performance in AWGN

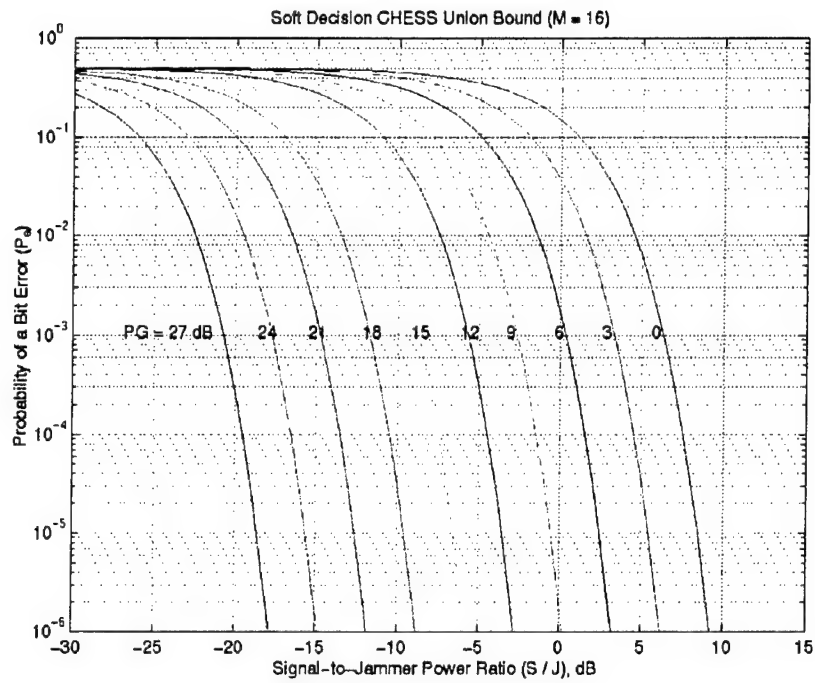


Figure B9. Soft Decision CHES Union Bound ($M = 16$) Performance in AWGN

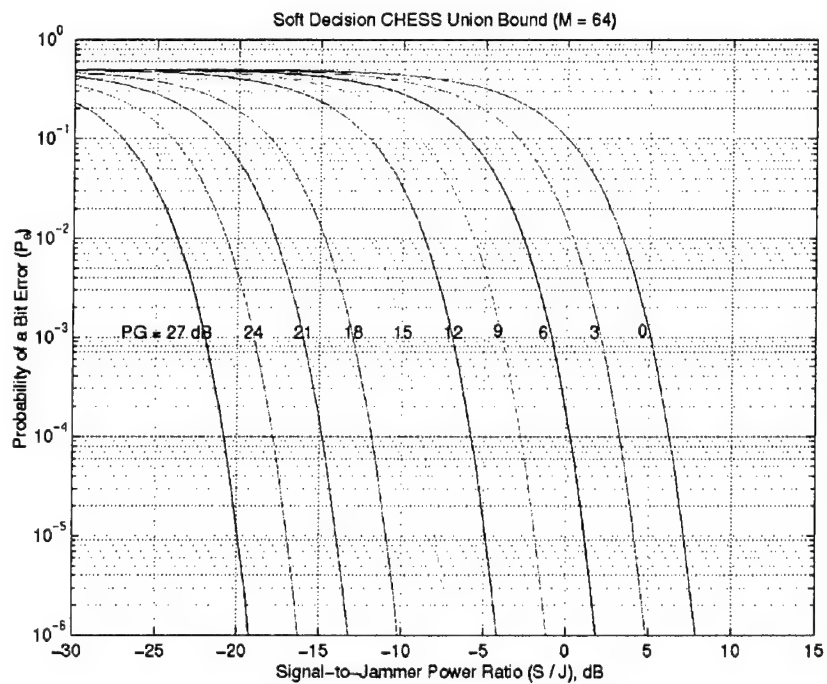


Figure B10. Soft Decision CHES Union Bound ($M = 64$) Performance in AWGN

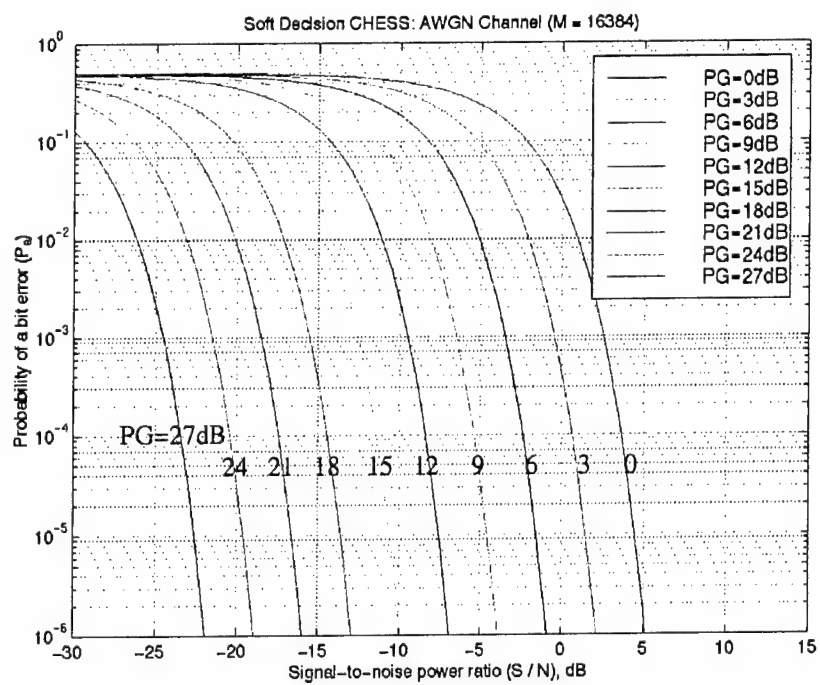


Figure B11. Soft Decision CHES Union Bound (M = 16384) Performance in AWGN

Rayleigh-Fading Channel Performance Curves

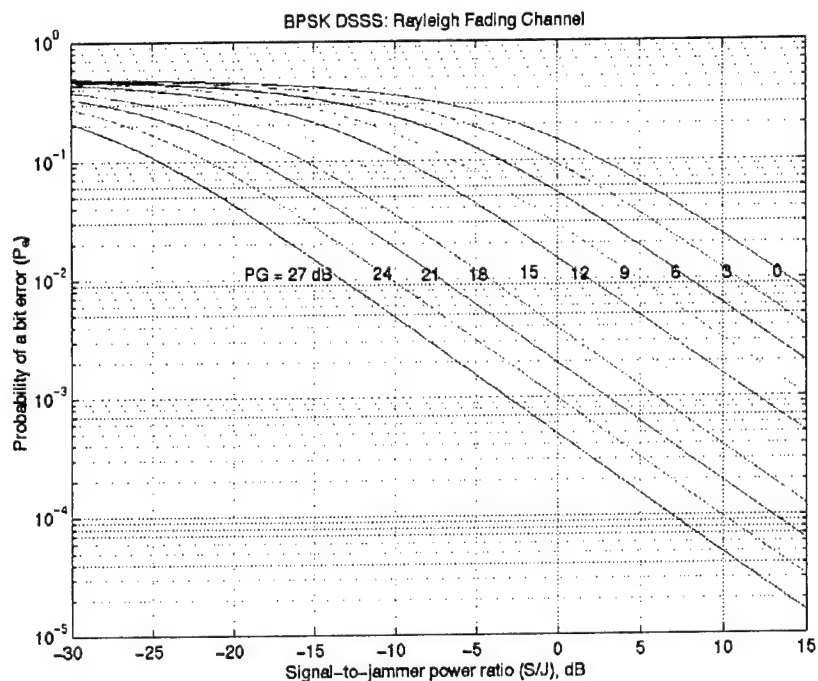


Figure B12. BPSK DSSS Performance in a Rayleigh Fading Channel

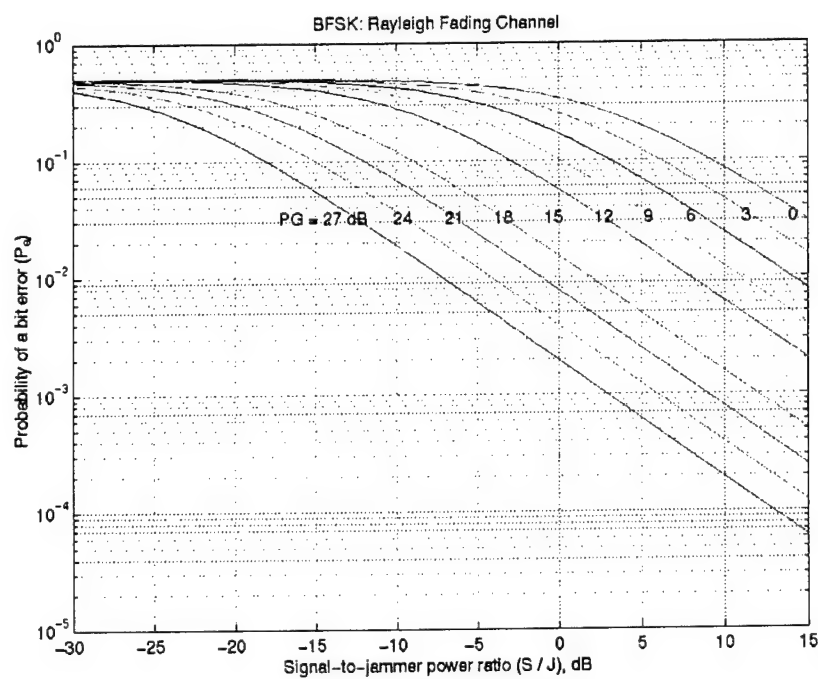


Figure B13. BFSK Performance in a Rayleigh Fading Channel

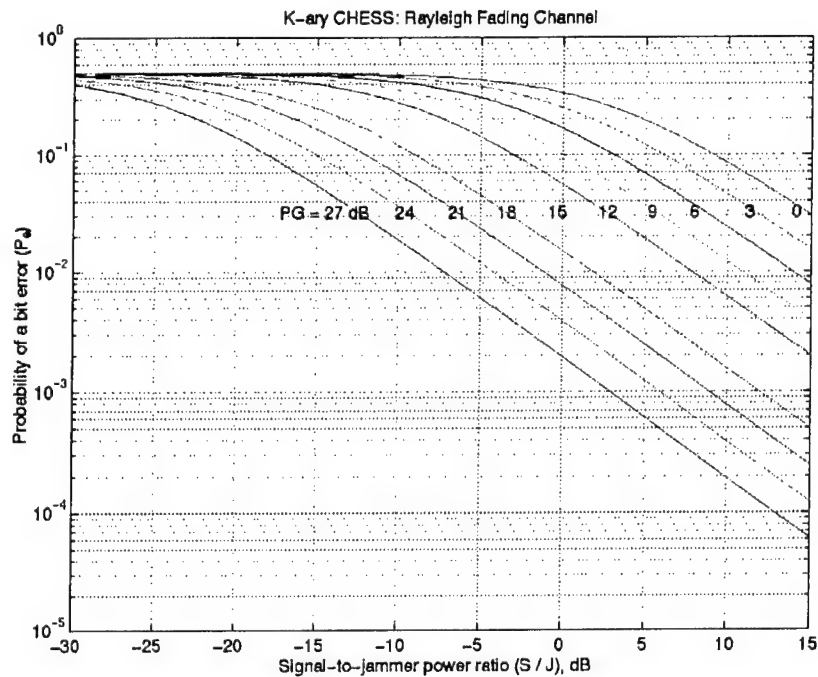


Figure B14. K-ary CHES Performance in a Rayleigh Fading Channel

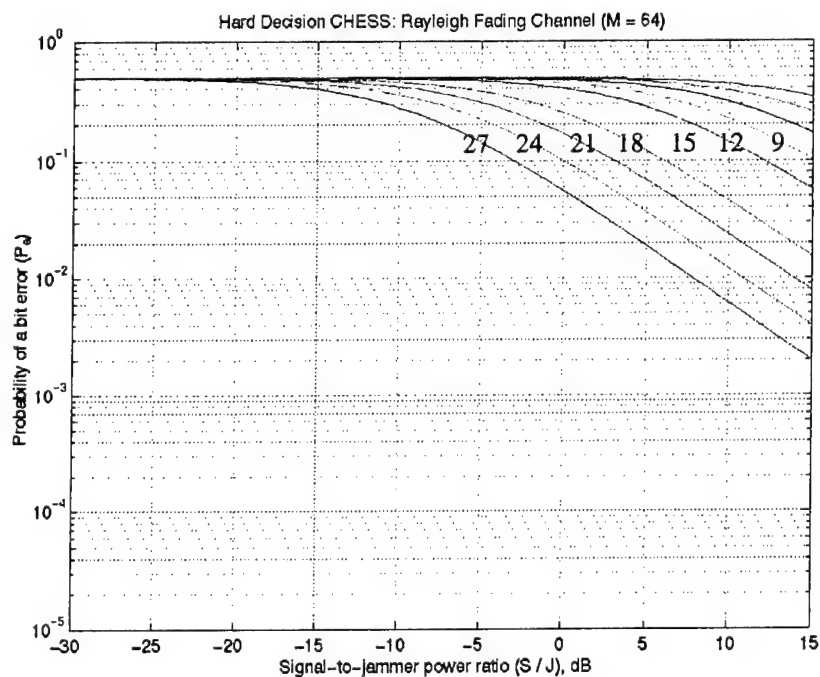


Figure B15. Hard Decision CHES ($M = 64$) Performance in a Rayleigh Fading Channel

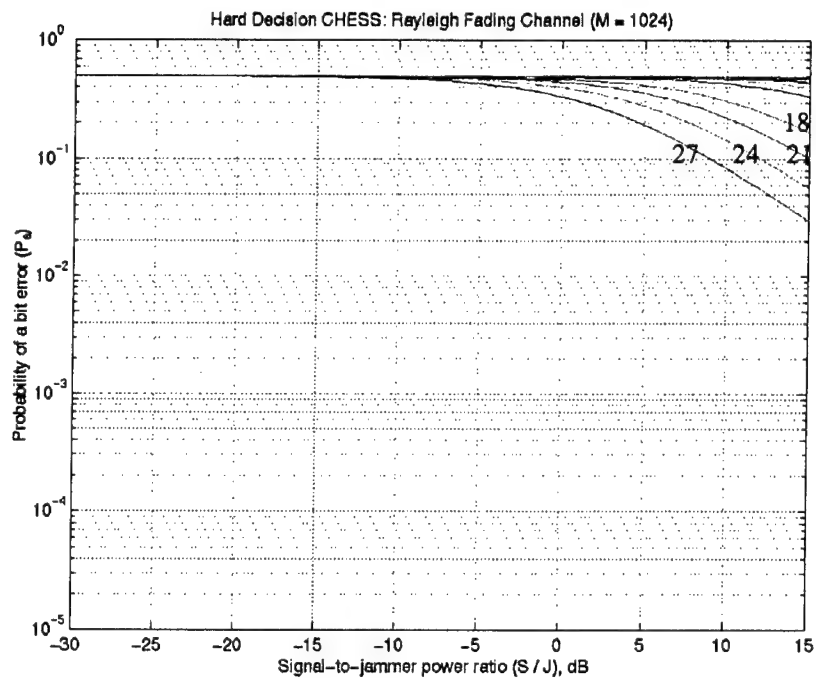


Figure B16. Hard Decision CHES ($M = 1024$) Performance in a Rayleigh Fading Channel

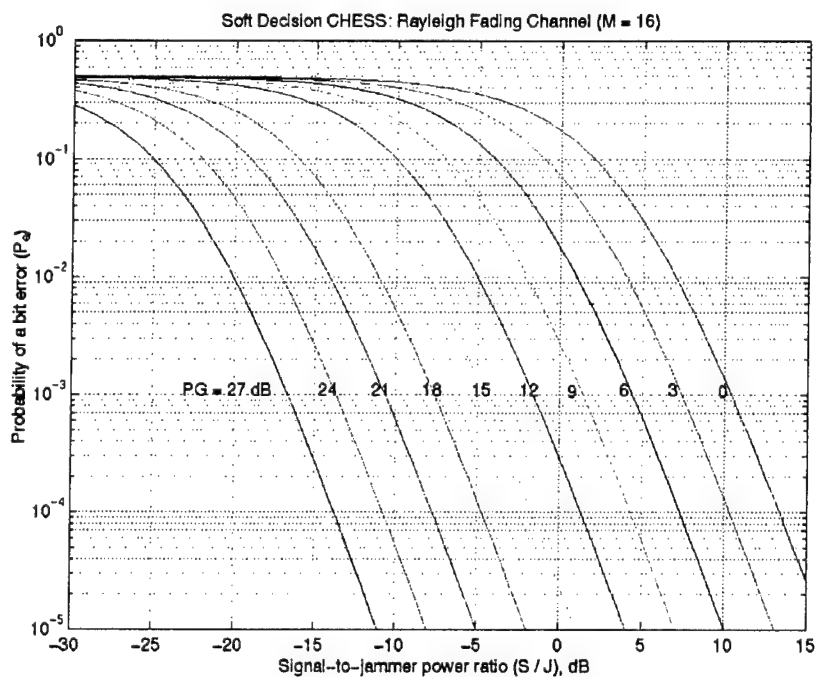
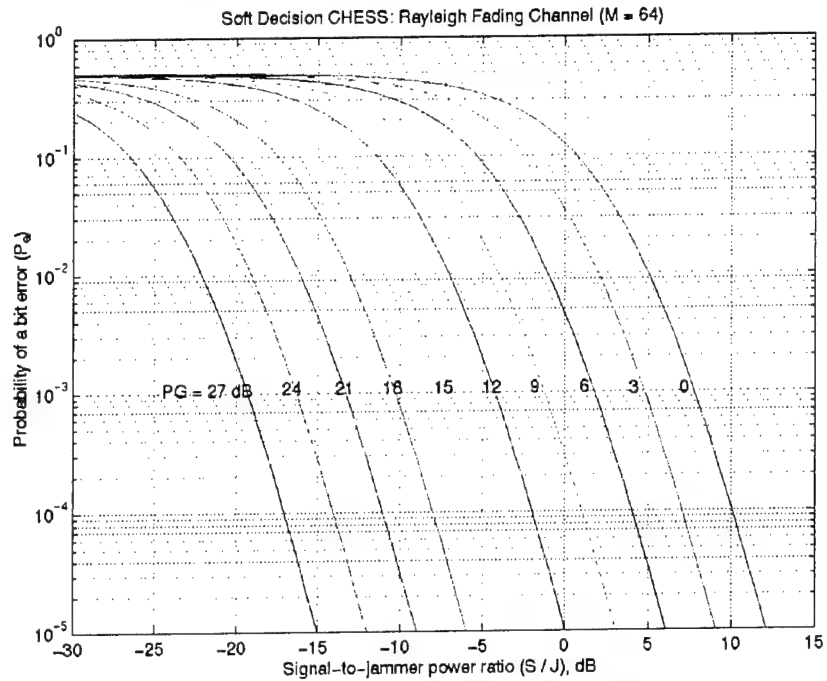
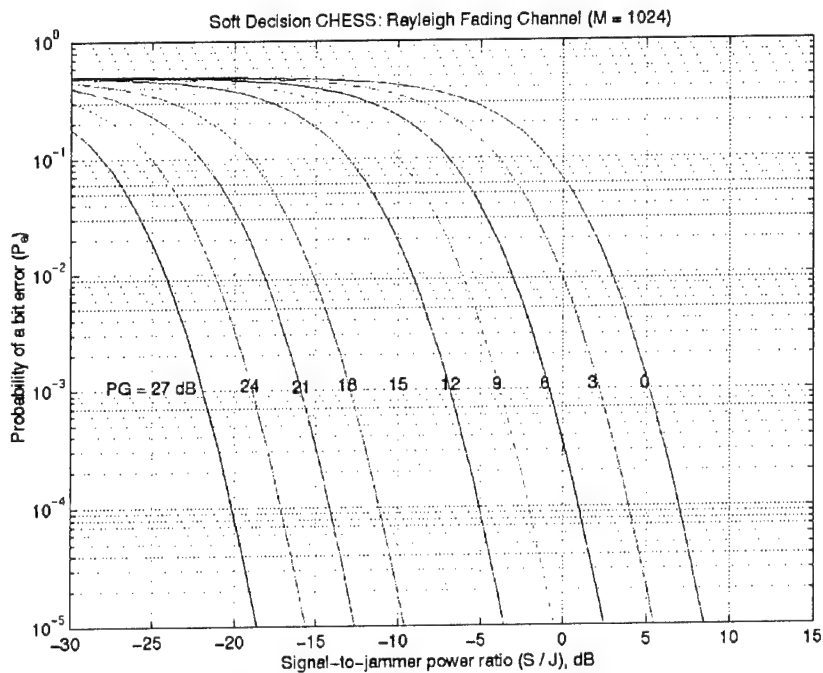


Figure B17. Soft Decision CHES Union Bound ($M = 16$) Performance in a Rayleigh Fading Channel



**Figure B18. Soft Decision CHES Union Bound ($M = 64$)
Performance in a Rayleigh Fading Channel**



**Figure B19. Soft Decision CHES Union Bound ($M = 1024$)
Performance in a Rayleigh Fading Channel**

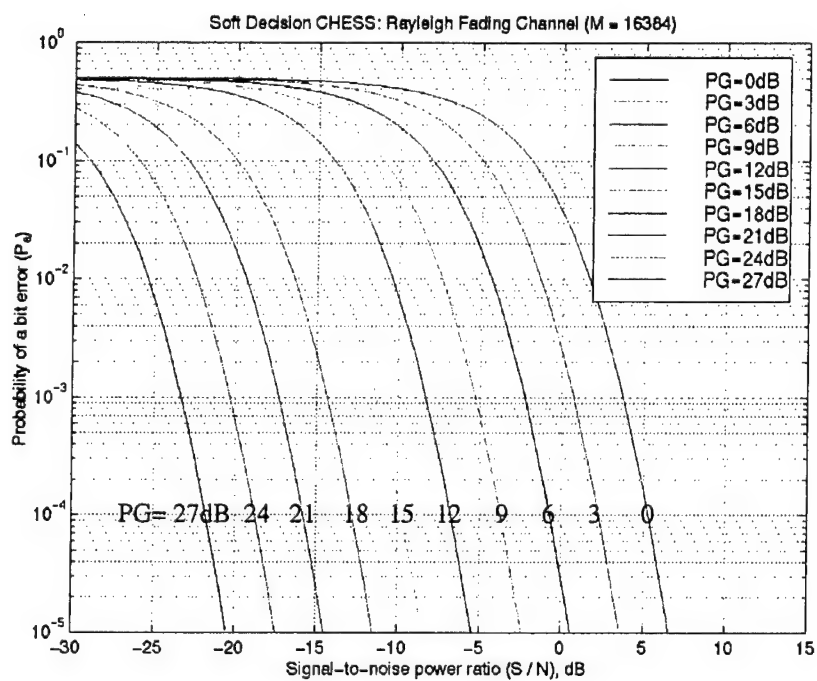


**Figure B20. Soft Decision CHES Union Bound (M = 16384)
Performance in a Rayleigh Fading Channel**

Appendix C: Intercept Performance in AWGN

Receiver Operating Characteristics (ROC) formulas

Detector Type	Basic Equation	Comments
Radiometer	$\frac{S}{N_0} = d \sqrt{\frac{W}{T}}$	<ul style="list-style-type: none"> • Provides lower bound on intercept performance • Most elementary and easy to implement receiver • Holds for large TW products (> 1000) • Independent of waveform type
Optimum Multichannel FH Pulse Matched ED	$\frac{S}{N} = \frac{1}{2N_T} I_0^{-1} \left[1 - N_T + N_T \exp\left(\frac{d^2 N_T}{WT}\right) \right]$	<ul style="list-style-type: none"> • LRT receiver for FH waveforms • Holds for > 100 hops • Assumes $W_h T_h = 1$
Synchronous Coherent Detector	$\frac{S}{N_0} = \frac{d}{2} \sqrt{\frac{W}{T}}$	<ul style="list-style-type: none"> • LRT receiver for DSSS waveforms • Assumes signal phase is known to the interceptor

Table C1. Intercept Performance Formulas

Radiometer (Wide-Band Energy Detector)

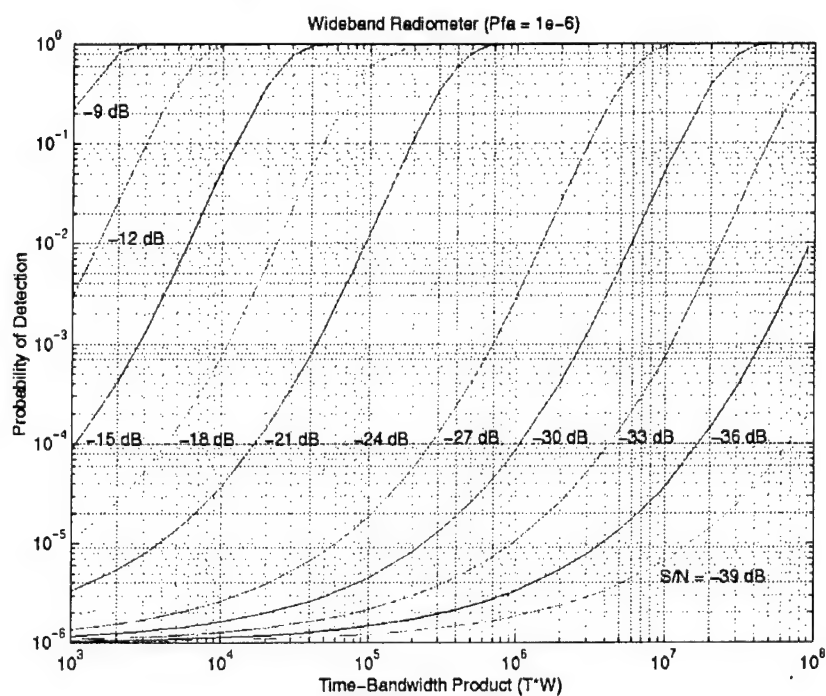


Figure C1. Radiometer Probability of Detection for $P_{fa} = 10^{-6}$

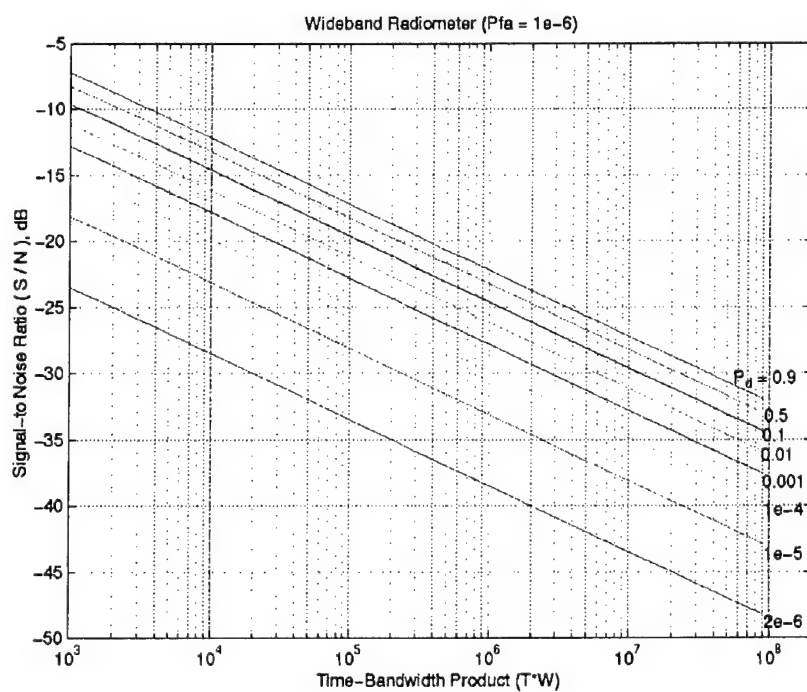


Figure C2. Radiometer Signal-to-Noise Power Ratio for $P_{fa} = 10^{-6}$

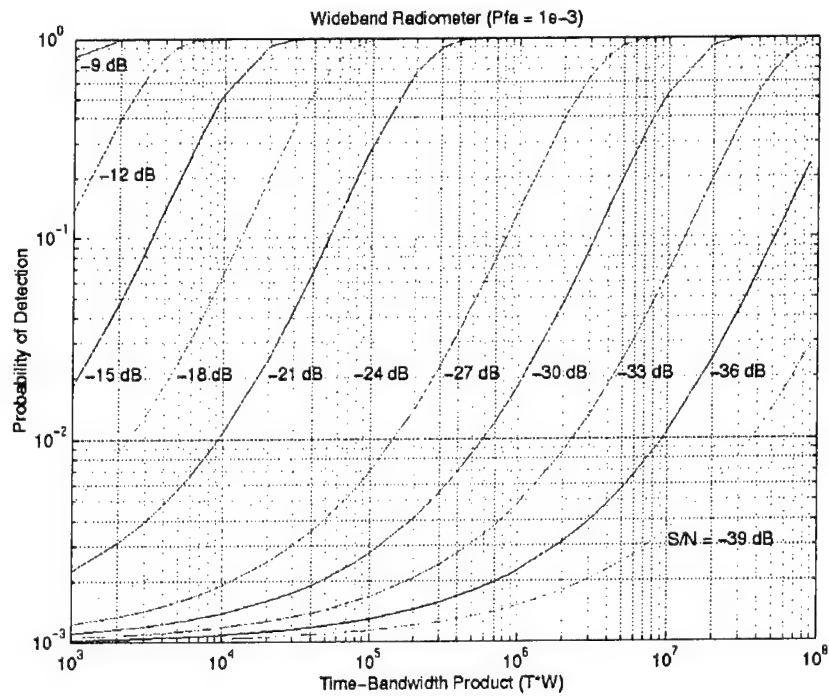


Figure C3. Radiometer Probability of Detection for $P_{fa} = 10^{-3}$

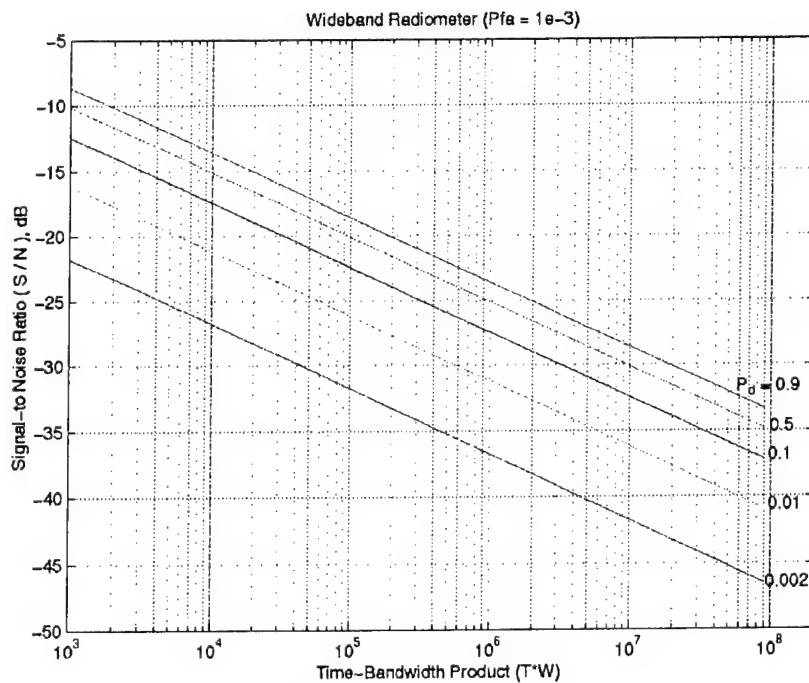


Figure C4. Radiometer Signal-to-Noise Power Ratio for $P_{fa} = 10^{-3}$

Optimum Multichannel FH Pulse Matched ED

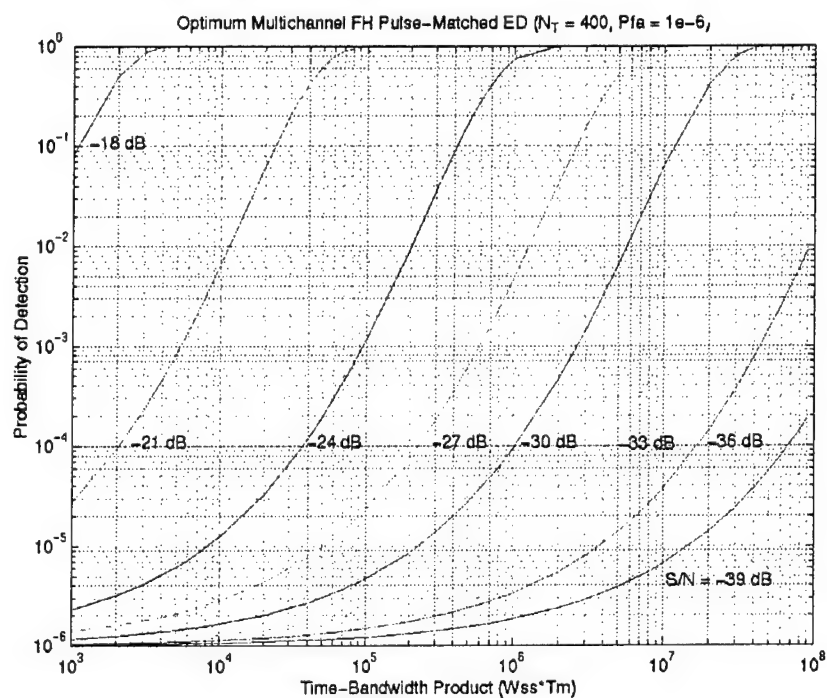


Figure C5. Optimum Multichannel FH Pulse-Matched Energy Detector
Probability of Detection for $P_{fa} = 10^{-6}$

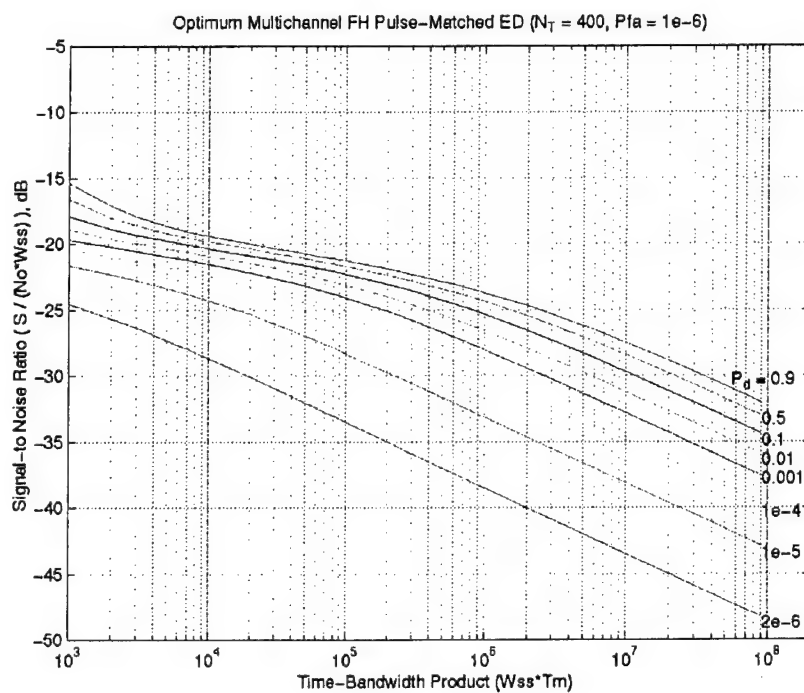


Figure C6. Optimum Multichannel FH Pulse-Matched Energy Detector
Signal-to-Noise Power Ratio for $P_{fa} = 10^{-6}$

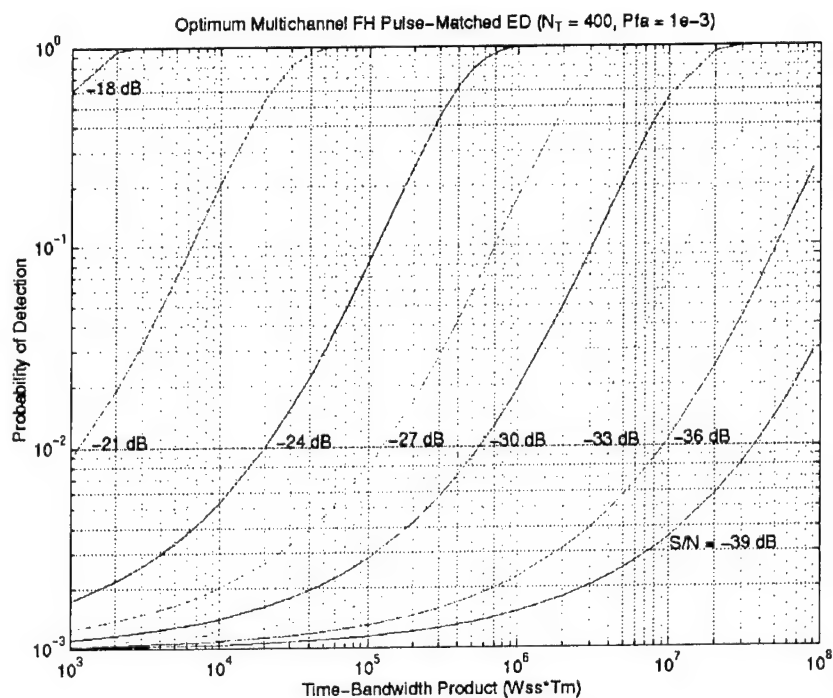


Figure C7. Optimum Multichannel FH Pulse-Matched Energy Detector
Probability of Detection for $P_{fa} = 10^{-3}$

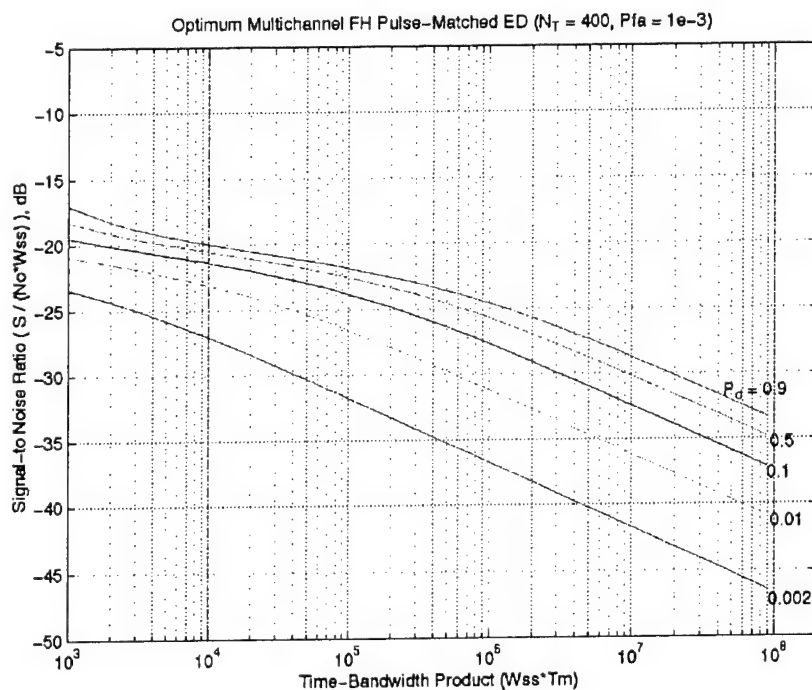


Figure C8. Optimum Multichannel FH Pulse-Matched Energy Detector
Signal-to-Noise Power Ratio for $P_{fa} = 10^{-3}$

Synchronous Coherent Detector

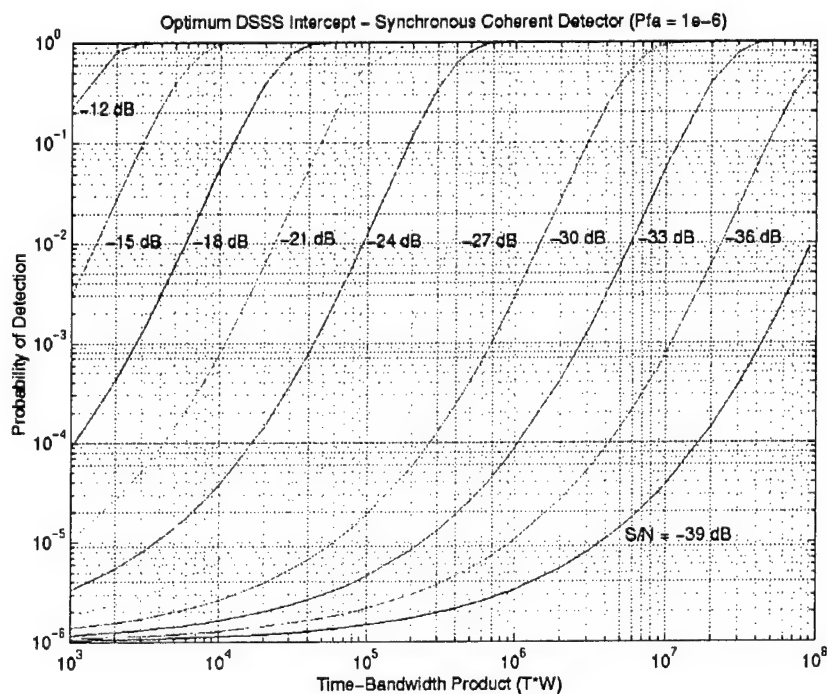


Figure C9. Synchronous Coherent Detector Probability of Detection for $P_{fa} = 10^{-6}$

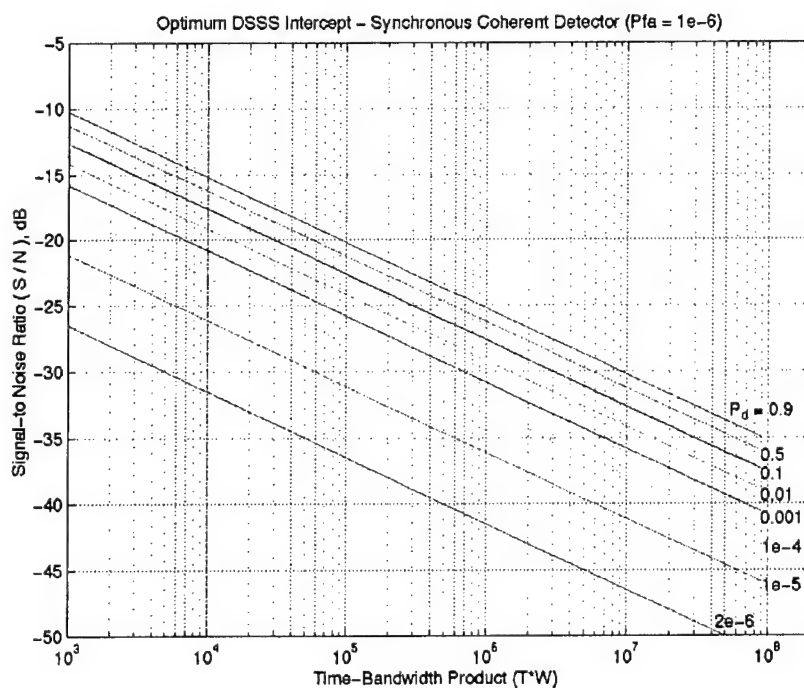


Figure C10. Synchronous Coherent Detector Signal-to-Noise Power Ratio for $P_{fa} = 10^{-6}$

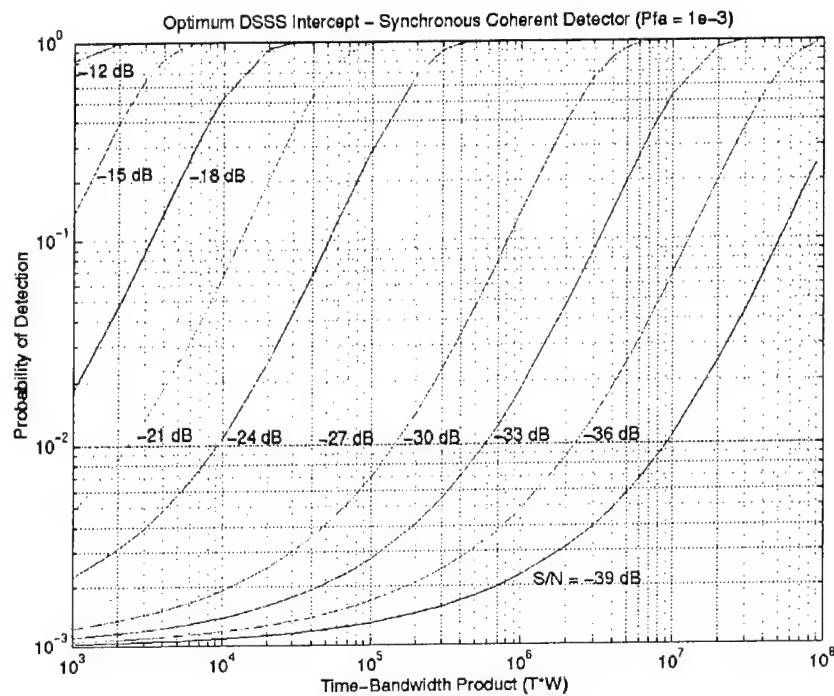


Figure C11. Synchronous Coherent Detector Probability of Detection for $P_{fa} = 10^{-3}$

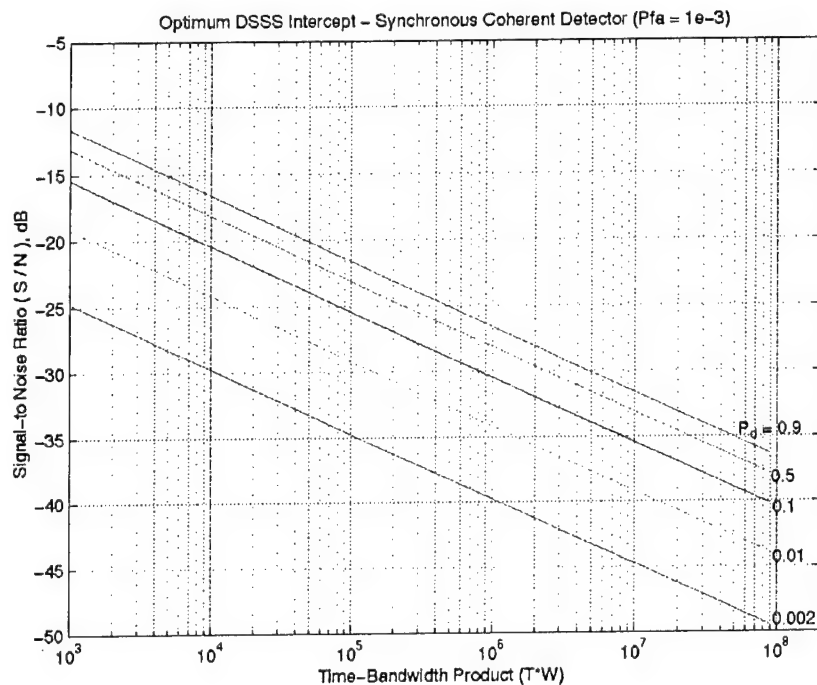


Figure C12. Synchronous Coherent Detector Signal-to-Noise Power Ratio for $P_{fa} = 10^{-3}$

Notation / Acronyms

A

ADCs	Analog-to-Digital Converters
AJ	Anti-Jam
AWGN	Additive White Gaussian Noise

B

bph	Bits Per Hop
bps	Bits Per Second
BER	Bit Error Rate
BPSK	Binary Phase Shift Keying
BW	Bandwidth

C

CDMA	Code-Division Multiple Access
CG	Coding Gain
CHES	Correlated Hopping Enhanced Spread Spectrum

D

d	Deflection Coefficient
d_{\min}^H	Minimum Hamming Distance
DACs	Digital-to-Analog Converters
dB	Decibel
DFH	Differential Frequency Hopping
DSSS	Direct Sequence Spread Spectrum

E

E_b	Energy per Bit
E_s	Energy per Symbol
ECC	Error Control Coding
ED	Energy Detector

F

f_0	Center Frequency
FDMA	Frequency-Division Multiple Access
FH	Frequency Hopped
FHSS	Frequency Hopped Spread Spectrum

G

γ	SNR per Symbol
γ_b	SNR per Bit
$\bar{\gamma}_b$	Average SNR per Bit

H

h	Bits per Hop
HD	Hard Decision
Hz	Hertz

I	
IBW	Instantaneous Bandwidth
J	
J	Jammer Power
J_0	Jammer PSD
K	
K	Number of Trellis Branches ($2^{b_{ph}}$)
kbps	Kilo Bits Per Second
kHz	KiloHertz
L	
L	Diversity Order ($\log_k M$)
L_c	Processing Gain, Spreading Factor
LPD	Low Probability of Detection
LPI	Low Probability of Interception
LRT	Likelihood Ratio Test
M	
M	Number of Frequencies
MAC	Multi-Access Control
MFSK	Multiple Frequency Shift Keying
MHz	MegaHertz
MOEs	Measures of Effectiveness
ms	Millisecond
N	
N	Noise Power
N_0	Noise PSD
N_c	Number of Conferenced Users
N_T	Number of Detector Channels
NB	Narrow-Band
O	
OFDM	Orthogonal Frequency Division Multiplexing
P	
P_D	Probability of Detection
P_e	Probability of a bit error
P_{fa}	Probability of False Alarm
P_J	Jammer Power
P_N	Noise Power
P_s	Signal Power
PG	Processing Gain
PSD	Power Spectral Density
PSK	Phase Shift Keying
Q	
QAM	Quadrature Amplitude Modulation
QPSK	Quadrature Phase Shift Keying

R	
R	Data Rate in bps
R_b	Data Rate in bps
R_c	Code Rate
R_s	Data Rate in sps
ROC	Receiver Operating Characteristics

S	
s	Seconds
S	Signal Power
SD	Soft Decision
SNPR	Signal-to-Noise Power Ratio (S/N)
SNR	Signal-to-Noise Ratio
sps	Symbols per Second

T	
T	Message (Signal) Duration
T_b	Bit Duration
T_c	Chip Duration
T_h	Hop Duration
TCM	Trellis Coded Modulation
TW	Time-Bandwidth

W	
W	Communications Signal Bandwidth
W_h	Hop Bandwidth
W_{ss}	Communications Signal Bandwidth
WB	Wide-Band

***MISSION
OF
AFRL/INFORMATION DIRECTORATE (IF)***

*The advancement and application of Information Systems Science
and Technology to meet Air Force unique requirements for
Information Dominance and its transition to aerospace systems to
meet Air Force needs.*